European Journal of Medicinal Chemistry 236 (2022) 114324

Contents lists available at ScienceDirect

European Journal of Medicinal Chemistry

journal homepage: http://www.elsevier.com/locate/ejmech

Discovery of spirooxadiazoline oxindoles with dual-stage antimalarial activity

Elizabeth A. Lopes [a], Raquel Mestre [a], Diana Fontinha [b], Jenny Legac [c], Jinxin V. Pei [d], Margarida Sanches-Vaz [b], Mattia Mori [e], Adele M. Lehane [d], Philip J. Rosenthal [c], Miguel Prudêncio [b], Maria M.M. Santos [a, *]

[a] Research Institute for Medicines (iMed.ULisboa), Faculty of Pharmacy, Universidade de Lisboa, Av. Prof. Gama Pinto, 1649-003, Lisboa, Portugal
[b] Instituto de Medicina Molecular João Lobo Antunes, Faculdade de Medicina da Universidade de Lisboa, Av. Prof. Egas Moniz, 1649-028, Lisboa, Portugal
[c] Department of Medicine, San Francisco General Hospital, University of California, San Francisco, CA, 94143, USA
[d] Research School of Biology, Australian National University, Canberra, ACT, 2601, Australia
[e] Department of Biotechnology, Chemistry and Pharmacy, University of Siena, Via Aldo Moro 2, 53100, Siena, Italy

ARTICLE INFO

Article history:
Received 17 November 2021
Received in revised form
24 March 2022
Accepted 25 March 2022
Available online 28 March 2022

Keywords:
Dual-stage antiplasmodial activity
Malaria
Oxadiazoline
Spirooxindoles
Resistance

ABSTRACT

Malaria remains a prevalent infectious disease in developing countries. The first-line therapeutic options are based on combinations of fast-acting artemisinin derivatives and longer-acting synthetic drugs. However, the emergence of resistance to these first-line treatments represents a serious risk, and the discovery of new effective drugs is urgently required. For this reason, new antimalarial chemotypes with new mechanisms of action, and ideally with activity against multiple parasite stages, are needed. We report a new scaffold with dual-stage (blood and liver) antiplasmodial activity. Twenty-six spirooxadiazoline oxindoles were synthesized and screened against the erythrocytic stage of the human malaria parasite *P. falciparum*. The most active compounds were also tested against the liver-stage of the murine parasite *P. berghei*. Seven compounds emerged as dual-stage antimalarials, with IC_{50} values in the low micromolar range. Due to structural similarity with cipargamin, which is thought to inhibit blood-stage *P. falciparum* growth via inhibition of the Na^+ efflux pump *Pf*ATP4, we tested one of the most active compounds for anti-*Pf*ATP4 activity. Our results suggest that this target is not the primary target of spirooxadiazoline oxindoles and further studies are ongoing to identify the main mechanism of action of this scaffold.

1. Introduction

Malaria is a hematoprotozoan infectious disease caused by *Plasmodium* parasites. In 2020, the WHO estimated that there were 241 million cases in 85 endemic countries, with the greatest burden in Africa. Malaria is particularly deadly in young children under 5, with about 77% of the 627 000 total malaria deaths estimated to occur in this age group in 2020. Other high-risk populations are pregnant women and non-immune travelers to malaria-endemic regions [1]. The bulk of serious morbidity and mortality from malaria is caused by *Plasmodium falciparum*, the most virulent human malaria parasite.

Malaria is transmitted by the bite of infected female *Anopheles* mosquitoes, which inject sporozoites into the skin of the mammalian host. Sporozoites travel to the liver and invade hepatocytes, where they replicate extensively without causing disease symptoms. Upon completion of this developmental process, merozoites released from hepatocytes enter the bloodstream and invade erythrocytes to begin the asexual bloodstream infection that is responsible for the clinical manifestations of malaria. Malaria therapy is directed against intraerythrocytic parasites. Activity against liver-stage parasites can prevent bloodstream infection, and thus offer chemoprevention against malarial illness [2].

Several drugs have been used to treat malaria (Fig. 1), but many of the available agents have been rendered less effective by the emergence of parasite resistance [3]. Currently, WHO guidelines recommend the use of artemisinin-based combination therapies (ACTs) to treat uncomplicated malaria [4–7]. However, resistance to artemisinin has emerged in Southeast Asia, and when resistance

* Corresponding author.
E-mail address: mariasantos@ff.ulisboa.pt (M.M.M. Santos).

https://doi.org/10.1016/j.ejmech.2022.114324
0223-5234/

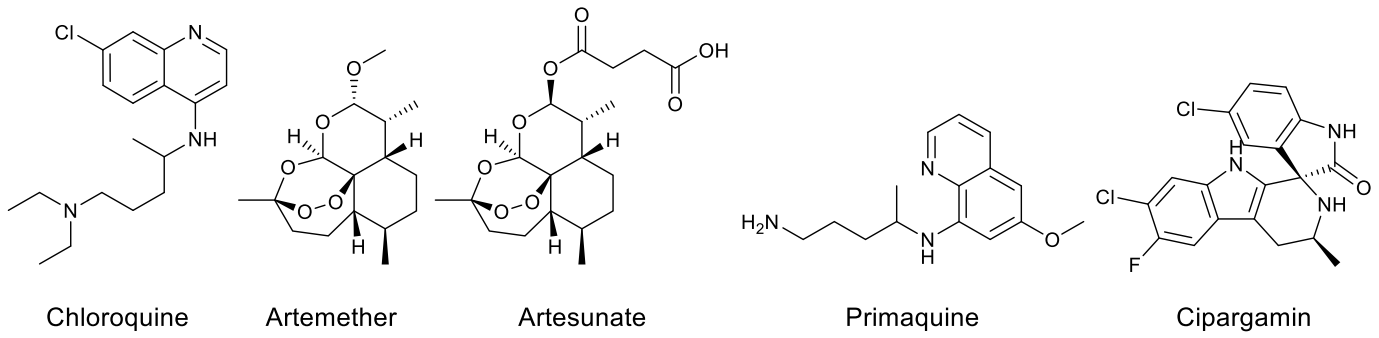

Fig. 1. Chemical structures of a selection of antimalarial drugs. Chloroquine was used as monotherapy in areas with chloroquine-susceptible infections. The artemisinin derivatives artemether and artesunate are used in ACTs. Primaquine is the first available drug to target the hepatic stage of the parasite life cycle. Cipargamin is an antimalarial with a previously unexploited mechanism of action – inhibition of the *Pf*ATP4 ion pump – that is undergoing clinical trials.

to both artemisinins and their partner drugs is observed, frequent treatment failures occur [8,9]. Many antimalarial drugs only target the asexual intraerythrocytic stage of the parasite. Some antimalarial drugs, such as primaquine and its derivative tafenoquine, also target the liver stage of the parasite, but these drugs have toxicity concerns [10]. Drugs targeting the liver-stage of infection can prevent bloodstream infection and might delay the development of parasite resistance [11,12]. Furthermore, the discovery and use of new chemical families that act against novel targets can circumvent resistance mechanisms that are already present or emerging in the field [13]. One compound that emerged as a promising antimalarial and is currently under clinical trials is cipargamin. This compound belongs to the spiroindolone class and acts against *P. falciparum* ATPase 4 (*Pf*ATP4), a novel parasite target [14–16].

Due to the interest in spirooxindoles as antimalarials and our interest in developing five-membered ring spirooxindoles for cancer therapy, we decided to explore the effects of spirooxadiazoline oxindoles against blood stage *P. falciparum* parasites and liver-stage *P. berghei* parasites [17–19]. This scaffold combines the indole and the oxadiazole moieties, which are important chemical structures in medicinal chemistry, due to their wide range of bioactivities [20,21]. In particular, the [1,3,4]-oxadiazole moiety, valuable in drug development due to its low lipophilicity, has been described as having antibacterial, antifungal, and insecticidal activities [22–25].

2. Results and discussion

To carry out a SAR study of this scaffold we prepared spirooxadiazoline oxindoles with the indole moiety unsubstituted (R^1 = H), or containing a halogen substituent (R^1 = Cl or Br) at positions 5, 6, and 7. The rationale was based on our previous results employing five-membered ring spirooxindoles and on reported results with spiroindolones, which showed halogens at positions 5 and/or 6 of the indole to be beneficial for bioactivity [14,15,26,27].

The effect on the antiplasmodial activity of different substituents on positions 2 and 4 (R^2 and R^3) of the oxadiazoline was also evaluated. Derivatives containing phenyl or substituted phenyl groups (with either activating or deactivating substituents), or a *t*-butyl group, with more conformational freedom, were prepared (Fig. 2).

Spirooxadiazoline oxindoles **1**–**26** (Table 1) were prepared by 1,3-dipolar cycloaddition reaction between isatin and nitrile imine derivatives, formed *in situ* by the dehydrochlorination of the corresponding hydrazonyl chloride, with 43–87% yields. The aromatic hydrazonyl chlorides were synthesized starting from hydrazine and

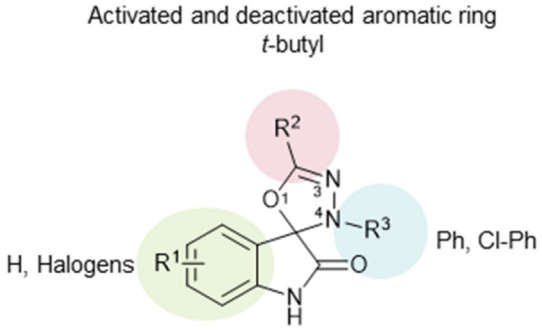

Fig. 2. Structural modifications for the design of spirooxadiazoline oxindole derivatives **1**–**26**.

benzaldehyde derivatives, followed by halogenation using the Corey-Kim reagent [28,29]. The alkyl-substituted hydrazonyl chlorides were prepared by reaction of pivaloyl chloride with different phenylhydrazine derivatives [30], followed by an Appel reaction (Scheme 1) [31].

The formation of the [1,3,4]-oxadiazole regioisomer in all reactions was confirmed by ^{13}C NMR, as the spiro carbon appears between 95 and 96 ppm, and the C=N at 152–154 ppm when R^2 is an aryl group and at 162–166 ppm when R^2 is an alkyl group, as previously reported for this regioisomer [32,33].

Compounds **1**–**26** were screened against blood-stage *P. falciparum* parasites (W2 strain, Table 1). Ten compounds displayed an IC_{50} lower than 10 μM (**9**, **13**–**14**, **16**, **18**–**19**, **23**–**26**), all bearing a halogen substituent on the oxindole moiety. Except for compound **9**, the most active compounds have a phenyl or a *t*-butyl group as R^2 substituent, and a *meta*-chlorophenyl or a *para*-chlorophenyl as R^3 substituent.

All compounds with hydrogen as R^1 substituent (**1**, **8**, **12**) or with *meta*-chloro (**1**–**4**, **20**) or *para*-chlorophenyl (**5**–**7**) as R^2 substituents were inactive. For derivatives with a 5-bromo R^1 substituent and a phenyl R^3 substituent, the presence of a *para*-methoxy phenyl R^2 substituent led to an active compound, with an IC_{50} value of 8 μM against the *P. falciparum* W2 strain (**9** versus **2** and **5**).

Moreover, the replacement of an aromatic ring by a *t*-butyl group as R^2 substituent also led to an at least 2-fold improvement in the activity of compounds containing a halogen at position 5 or 6 of the oxindole and a *meta*-chlorophenyl as R^3 substituent (**14**–**16** versus **24**–**26**). The type of halogen at positions 5 or 6 of the oxindole also appeared to be important for activity, as H, 6-Br, and 7-Cl as R^1 substituents led to inactive compounds (**13**–**14** and **16** versus **12**, **15,** and **17**). The type of halogen and position of the

Table 1
Yields and antiplasmodial activities of compounds **1**–**26**.

Compound	R^1	R^2	R^3	Yield	*Pf* W2[a] IC_{50} (μM)	*Pb*[b] IC_{50} (μM)
1	H	*m*-Cl-Ph	Ph	80%	>10	ND
2	5-Br	*m*-Cl-Ph	Ph	61%	>10	ND
3	5-Cl	*m*-Cl-Ph	Ph	85%	>10	ND
4	7-Cl	*m*-Cl-Ph	Ph	54%	>10	ND
5	5-Br	*p*-Cl-Ph	Ph	51%	>10	ND
6	5-Cl	*p*-Cl-Ph	Ph	64%	>10	ND
7	7-Cl	*p*-Cl-Ph	Ph	67%	>10	ND
8	H	*p*-OMe-Ph	Ph	42%	>10	ND
9	5-Br	*p*-OMe-Ph	Ph	61%	8.3 ± 0.7	>10
10	5-Cl	*p*-OMe-Ph	Ph	63%	>10	ND
11	7-Cl	*p*-OMe-Ph	Ph	53%	>10	ND
12	H	Ph	*m*-Cl-Ph	87%	>10	ND
13	5-Br	Ph	*m*-Cl-Ph	64%	6.7 ± 0.9	3.9 ± 0.1
14	5-Cl	Ph	*m*-Cl-Ph	64%	6.4 ± 0.4	7.0 ± 1.4
15	6-Br	Ph	*m*-Cl-Ph	78%	>10	ND
16	6-Cl	Ph	*m*-Cl-Ph	43%	8.6 ± 0.2	7.2 ± 1.7
17	7-Cl	Ph	*m*-Cl-Ph	68%	>10	ND
18	5-Br	Ph	*p*-Cl-Ph	74%	6.0 ± 0.5	4.1 ± 0.3
19	7-Cl	Ph	*p*-Cl-Ph	68%	7.6 ± 0.1	>10
20	7-Cl	*m*-Cl-Ph	*m*-Cl-Ph	67%	>10	ND
21	5-Br	*t*-Bu	*o*-Cl-Ph	65%	>10	ND
22	5-Cl	*t*-Bu	o-Cl-Ph	65%	>10	ND
23	5-Br	*t*-Bu	*m*-Cl-Ph	70%	7.5 ± 1.8	9.0 ± 1.5
24	5-Cl	*t*-Bu	*m*-Cl-Ph	64%	3.5 ± 0.1	5.3 ± 0.1
25	6-Br	*t*-Bu	*m*-Cl-Ph	53%	4.6 ± 0.4	9.5 ± 0.1
26	6-Cl	*t*-Bu	*m*-Cl-Ph	80%	3.8 ± 0.02	>10

[a] The blood-stage antiplasmodial activity was determined for chloroquine-resistant *P. falciparum* (*Pf*) parasites (W2 strain). Data represent the mean ± SD of two independent experiments.
[b] Liver-stage antiplasmodial activity was determined in *P. berghei* (*Pb*). Data represent the mean ± SD of three independent experiments. ND − not determined.

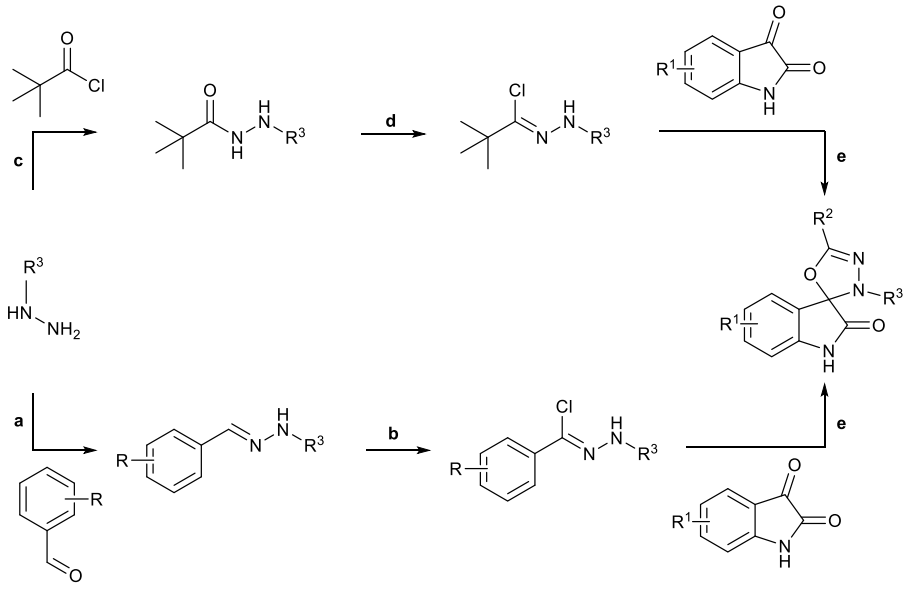

Scheme 1. Synthetic route used to prepare spirooxadiazoline oxindoles. a) 20% aqueous EtOH, r.t., 3h, dark; b) NCS, SMe_2, CH_2Cl_2, -78 °C, 1h; c) Et_3N, THF, r.t., 18h; d) PPh_3, CCl_4, CH_3CN, r.t., 16h; e) R^2 = *t*-butyl or R-substituted phenyl; NEt_3, CH_2Cl_2, r.t., 16h.

oxindole substituted was also important for the activity of compounds with a methoxyphenyl as R^2 substituent (**8**-**11**).

The most active compounds against the blood-stage of the *P. falciparum* parasites were also evaluated for their ability to inhibit hepatic infection by the rodent malaria parasite *P. berghei* (Table 1 and Fig. 3). Of the ten compounds tested, seven showed dual-stage activity, with IC_{50} values ranging from 3.5 to 9.5 μM against *P. berghei* hepatic infection. Compound **19**, with a 7-chlorooxindole moiety, and compound **9**, with a *para*-methoxy phenyl as R^2 substituent, were not active against hepatic *P. berghei* parasites.

With the aim to obtain insights into the possible mechanism of action of these spirooxadiazoline oxindole derivatives, a ligand-based molecular modeling study was carried out. Specifically, we compared the chemical and shape features of our active compounds with those of known antimalarial compounds using the Tanimoto Combo similarity index (TC).

A library of known antimalarial compounds was downloaded from the DrugBank database [34], and conformations of each

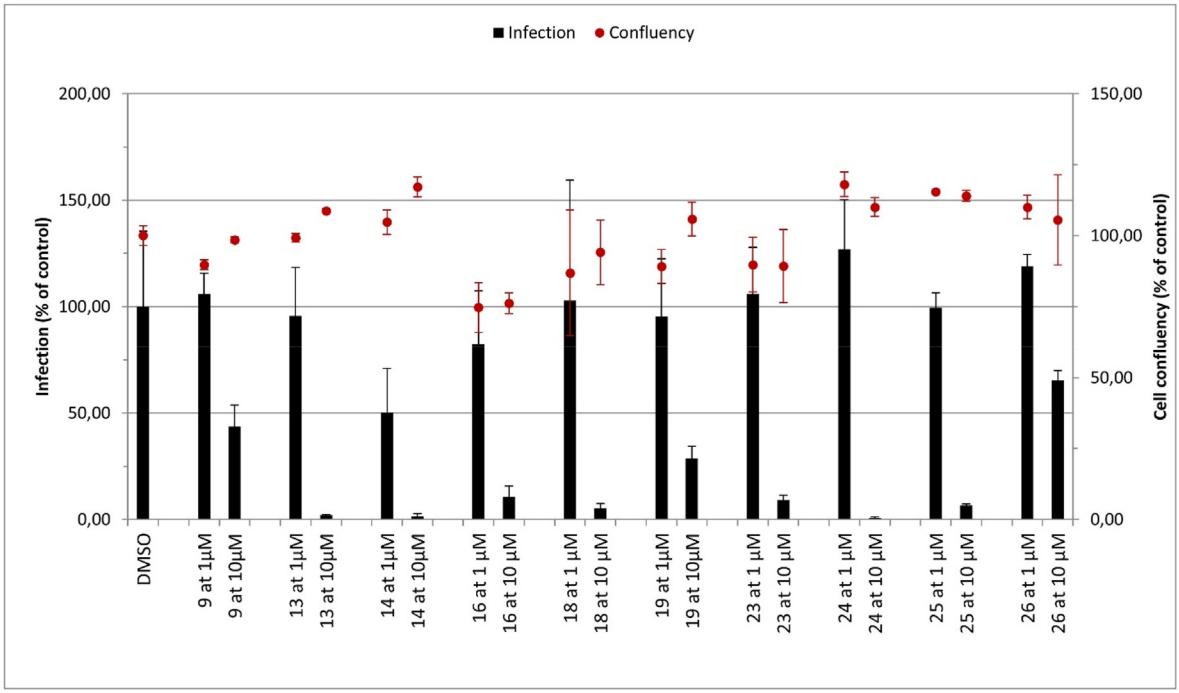

Fig. 3. Luminescence-based activity (bars) of compounds **9**, **13**–**14**, **16**, **18**–**19,** and **23**–**26** against infection of Huh7 cells by luciferase-expressing *P. berghei* and compound toxicity (dots) assessed by the confluence of Huh7 cells. Compounds were not toxic for uninfected mammalian cells.

antimalarial drug were generated to compute the shape and chemical similarities between our bioactive compounds (**9**, **13**–**14**, **16**, **18**–**19**, **23**–**26**) and the reference drugs. ROCS results highlighted the five top-ranking drugs with a relatively high TC score, i.e., cipargamin, clotrimazole, artemotil, arteninol, and artemether (Table 2), with the spiroindolone cipargamin displaying around 62% similarity with the bioactive spirooxadiazoline oxindoles reported here. From a conformational and structural standpoint, cipargamin and the most promising compounds (Fig. 4) have an overlapping oxindole moiety. The unique structural conformation of the spiro carbon is likely responsible for the occupation of the same space by the 1,2,3,6-tetrahydropyridine of cipargamin and the (1,3,4)-oxadiazole ring. Moreover, the substituents of these two moieties are partially overlapped. The methyl group of cipargamin is projected to occupy the same region as the *t*-butyl group of **24** and **25**, while the *meta*-chlorophenyl group perfectly overlaps with the same moiety of the indole-fused ring. For compounds **14** and **18**, with aromatic substituents, the overlapping inverts as the *meta*-chlorophenyl group is superimposed to the methyl group of the cipargamin and the phenyl group overlaps with the indole-fused ring of cipargamin.

Overall, molecular modeling raised the possibility that the spirooxadiazoline oxindole derivatives might share the same target and mechanism of action with cipargamin, which consists in the P-type cation-translocating ATPase *Pf*ATP4 inhibition [15]. *Pf*ATP4 has been proposed to function as an ATP-dependent Na^+/H^+ pump, extruding Na^+ ions from the parasite cytosol while importing H^+ ions [16]. To investigate whether spirooxadiazoline oxindoles inhibit *Pf*ATP4 we examined the effects of **18** on (1.) the parasite's cytosolic Na^+ concentration and (2.) the cipargamin-sensitive Na^+-ATPase activity present in *P. falciparum* membrane preparations. In Na^+ assays, saponin-isolated trophozoite-stage *P. falciparum* parasites (3D7 strain) were loaded with the Na^+-sensitive fluorescent dye SBFI (more detail on the method can be found in Ref. [16]). No increase in the parasite's cytosolic $[Na^+]$ was observed when parasites were exposed to **18** concentrations $\leq$20 μM (not shown). We then evaluated **18** at a concentration of 50 μM over a 90 min period (Fig. 5). As expected, cipargamin (positive control; tested at 50 nM) gave rise to an immediate-onset gradual increase in the parasite's cytosolic $[Na^+]$. However, **18** did not affect the parasite's cytosolic $[Na^+]$. We confirmed that the **18** used in the Na^+ assays was active against the 3D7 strain of *P. falciparum* in 72 h parasite proliferation assays (using a previously described method [35], $IC_{50} = 6.2 \pm 0.1$ μM (mean ± range/2; n = 2)).

We also tested the effect of **18** (at 50 μM) in a cell-free assay for *Pf*ATP4 activity. We measured the amount of P_i produced as a result of ATP hydrolysis in membranes prepared from isolated 3D7 parasites under high-$[Na^+]$ (152 mM) and low-$[Na^+]$ (2 mM) conditions and in the presence and absence of cipargamin (250 nM). The cipargamin-sensitive, Na^+-dependent fraction of membrane ATPase activity is used as a proxy for *Pf*ATP4 activity [36]. As expected, the positive control cipargamin inhibited the Na^+-dependent fraction of membrane ATPase activity (Fig. 6). When applied directly to parasite membrane preparations at 50 μM, **18** was found to inhibit both Na^+-dependent and Na^+-independent membrane ATPase activity (Fig. 6), consistent with **18** inhibiting *Pf*ATP4 (and at least one other membrane ATPase) at 50 μM. These findings suggest that spirooxadiazoline oxindoles have some activity against *Pf*ATP4 at high concentrations.

It has been found previously that spiroindolones inhibit Na^+-dependent ATPase activity in membrane preparations at lower concentrations than those required to dysregulate cytosolic $[Na^+]$

Table 2
Top 5 ranking TC score results from the shape and chemical similarity screening.

TC	Antimalarial	Similarity	Spirooxadiazoline oxindole
1.267	Cipargamin	62%	**14**
0.963	Clotrimazole	48%	**24**
0.912	Artemotil	46%	**26**
0.910	Artenimol	45%	**26**
0.900	Artemether	45%	**26**

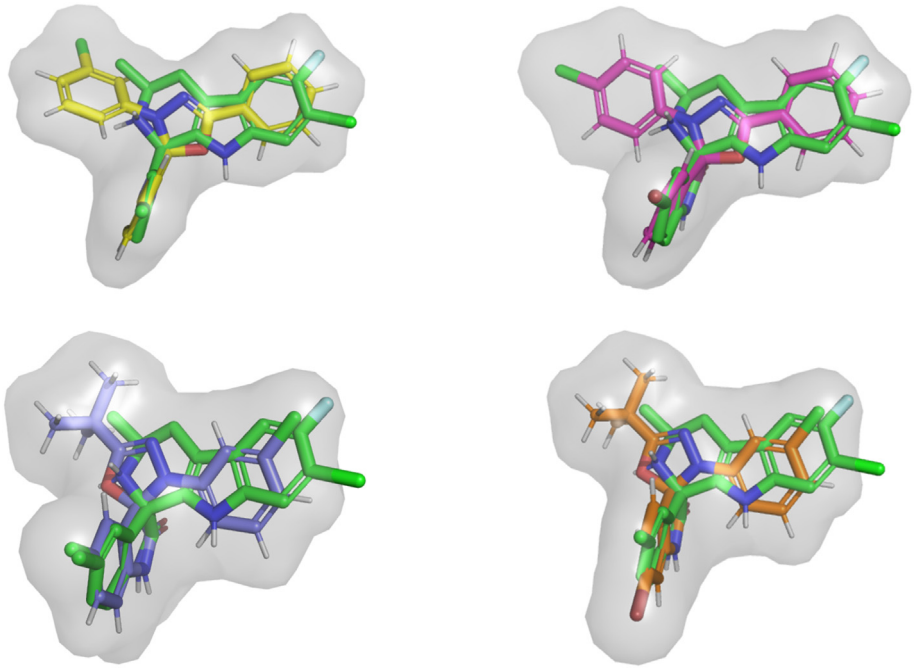

Fig. 4. Chemical and shape comparison of cipargamin (green sticks) and spirooxadiazoline oxindoles **14** (yellow sticks), **18** (pink sticks), **24** (blue sticks), and **25** (orange sticks). The molecular shape of the spirooxadiazoline oxindoles is shown as a grey transparent surface.

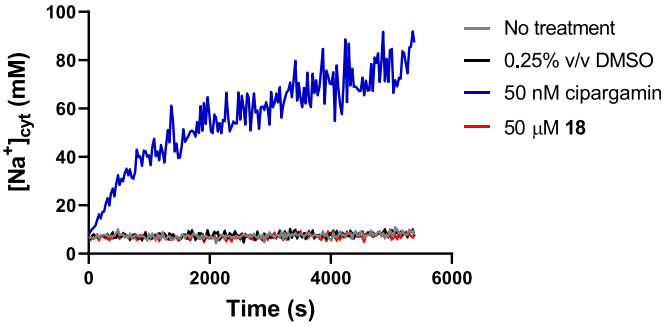

Fig. 5. Effect of the spirooxadiazoline oxindole **18** (50 μM) on cytosolic [Na^+] ([Na^+]$_{cyt}$) in isolated SBFI-loaded 3D7 parasites suspended in a physiological saline solution at 37 °C. Cipargamin (50 nM; positive control) and DMSO (0.25% v/v; solvent control) were tested in parallel. The data are from a single experiment and are representative of those obtained in three similar experiments.

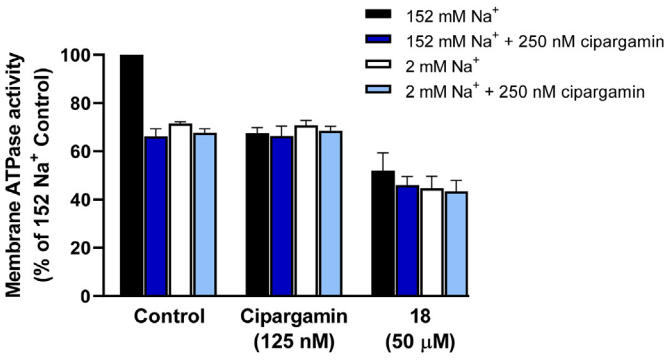

Fig. 6. Effect of the spirooxadiazoline oxindole **18** (50 μM) on ATPase activity in membranes prepared from *P. falciparum* parasites (3D7 strain) under high-[Na^+] (152 mM) and low-[Na^+] (2 mM) conditions, and in the presence and absence of cipargamin (250 nM). An equivalent concentration of solvent (DMSO) alone (Control) and cipargamin (125 nM) were tested in parallel. The data are the mean +SEM from three independent experiments, each performed on different days with different membrane preparations.

in live parasites [16]. Thus, even though 50 μM of **18** was sufficient to cause near-complete inhibition of Na^+-dependent ATPase activity in membrane preparations, concentrations of **18** higher than 50 μM may be required to cause a detectable increase in cytosolic [Na^+]. Nevertheless, in light of previous studies with *Pf*ATP4 inhibitors [16,37–39], the findings that, at a concentration of **18** that is > 8-fold higher than its IC_{50} for inhibition of parasite growth, the inhibition of Na^+-dependent membrane ATPase activity did not appear to be complete, and an increase in cytosolic [Na^+] was not detectable suggests that ATP4 might not be the primary or the only target modulated by spirooxadiazoline oxindoles and that these molecules might have a mechanism of action different from that of cipargamin. Further studies will be carried out to clarify this issue. Of note, 28 chemically diverse antiplasmodial compounds that display the biochemical hallmarks of *Pf*ATP4 inhibition have been tested for their ability to inhibit *P. berghei* liver-stage infection, and none of these were found to be liver-stage and blood-stage 'double actives' [40]. Furthermore, the most clinically advanced *Pf*ATP4 inhibitor, cipargamin, does not display activity against liver stage parasites [41,42]. Thus, the finding that many of the spirooxadiazoline oxindoles have similar activities against *P. falciparum* blood-stage and *P. berghei* liver-stage parasites also suggests that ATP4 is not the primary target of these compounds.

3. Conclusion

Here we described the discovery of novel spirooxadiazoline oxindoles with dual-stage antiplasmodial activity. The new derivatives were synthesized by 1,3-dipolar cycloaddition of isatin as dipolarophiles and nitrile imine derivatives as dipoles with moderate to high yields. Structural modifications were studied such as

the introduction of halogens in different positions of the oxindole moiety and aromaticity of the substituents of the oxadiazole ring and the new derivatives were evaluated against blood-stage chloroquine-resistant *P. falciparum* and liver-stage *P. berghei* parasites. The most active compounds, with IC_{50} below 10 μM, had a halogen at positions 5 and 6 at the oxindole moiety, phenyl, or *t*-butyl groups at position 2 of the oxadiazole ring and *meta*-chlorophenyl group at position 4 of this latter ring. Additionally, *in silico* ligand-based molecular modeling study was performed to provide insights into the possible mechanism of action of these compounds, using the TC. From this study, cipargamin was the drug with the highest TC (up to 62% similarity) which raised the possibility that spirooxadiazoline oxindole derivatives inhibit the protein *Pf*ATP4, like cipargamin. Further biological studies were carried out to investigate whether *Pf*ATP4 was the target of the spirooxadiazoline oxindole derivatives. Compound **18** was used in this study (60% similarity, see Supporting Information). In cell-free assays, this compound inhibited both Na^+-dependent and Na^+-independent membrane ATPase activity at 50 μM, suggesting that compound **18** inhibits *Pf*ATP4 and one or more other membrane ATPases. Despite some evidence for inhibition of *Pf*ATP4 at high concentrations, the inhibition of this protein does not seem to be the primary mechanism of action of our active compounds and further studies will be carried out to enlighten the target of the spirooxadiazoline oxindoles.

4. Experimental section

4.1. Chemistry

4.1.1. General information

All chemicals were obtained from commercial suppliers and used without prior purification. Dichloromethane, triethylamine, and tetrahydrofuran were distilled from calcium hydride, potassium hydroxide, and sodium-benzophenone system, respectively. For monitoring the reactions, Merck Silica Gel 60 F254 aluminum plates were used and visualized at 254 nm UV light. Compounds were purified using Panreac Aplichem Silica Gel 60 (40–63 μm) or Merck Silica Gel 60 GF254.

The infrared spectra were collected on a Shimadzu FTIR Affinity-1 spectrophotometer. The spectra were determined using thin films in a NaCl pellet. Only the most significant absorption bands are reported.

^{1}H NMR and ^{13}C NMR spectra were recorded at 300 MHz and 75 MHz, respectively, at 297 K, on a Bruker 300 MHz/54 mm Ultra-Shield Spectrometer (Wissenbourg, Bas-Rhin, France). The chemical shifts are reported in parts per million (ppm, δ) referenced to acetone-d_6 (VWR Chemicals, 99.80% D), while the proton coupling constants *J* in Hertz (Hz). Multiplicities are given as s (singlet), br s (broad singlet), d (doublet), dd (double doublet), ddd (double of double doublet), td (triplet of doublets), t (triplet), and m (multiplet).

Melting points were determined using a Kofler camera Bock monoscope M.

LC-DAD-MS experiments were carried out with Waters Alliance 2695 HPLC with a Sunfire C18 column (100 × 2.1 mm; 5 μm) at 35 °C, using an isocratic binary solvent system of CH_3CN:H_2O (70:30 v/v%) with a flow rate of 1 mL/min, with a photodiode array detector to scan wavelength absorption from 230 to 650 nm and interfaced with a triple quadrupole mass Spectrometer MicroMass Quattromicro® API (Waters®, Ireland) with an electrospray in positive ion mode (ESI+), ion source at 120 °C, a capillary voltage of 3.0 kV and the source voltage of 30V (Mass Spectrometry Laboratory, Faculty of Pharmacy of Lisbon University). Elemental analysis (C, H, and N) was performed in a FLASH 2000 Series by Thermo Scientific. The results were within ±0.5% of the theoretical values.

The intermediates hydrazones, hydrazides, and hydrazonyl chlorides were synthesized according to the literature [28–31].

4.1.2. General procedure for the synthesis of spirooxadiazoline oxindoles derivatives

Triethylamine (2.0 equiv) was added dropwise to a mixture of isatin derivative (50 mg, 1.0 equiv) and hydrazonyl chloride derivative (2.0 equiv) in dichloromethane (1 mL/0.1 mmol of isatin) at room temperature, under nitrogen atmosphere. After consumption of the limiting reagent, the reaction mixture was quenched with distilled water. The aqueous phase was separated, and the organic phase was washed with brine twice (2 × 10 mL). The combined organic extracts were dried over anhydrous Na_2SO_4, and the solvent was removed under vacuum. The crude was purified by chromatography using eluent *n*-hexane:ethyl acetate, followed by recrystallization in CH_2Cl_2/*n*-heptane affording the respective spirooxadiazoline oxindole.

5'-(3-chlorophenyl)-3′-phenyl-3′H-spiro[indoline-3,2'-[1,3,4]**oxadiazol]-2-one 1:** Reaction time: 16 h. Yield: 80%, yellow solid, mp 216–217 °C. **IR** (NaCl, selected peaks) ν_{max} (cm^{-1}) 3280 (NH), 1737 (C=O), 1600 (C=N). **^{1}H-NMR** (300 MHz, Acetone-d_6) δ 10.00 (s, 1H, NH), 7.88–7.81 (m, 2H, ArH), 7.60–7.49 (m, 4H, ArH), 7.23–7.13 (m, 4H, ArH), 7.64–6.79 (m, 3H, ArH).**^{13}C NMR** (75 MHz, acetone-d_6) δ 172.4 (C=O), 152.3 (C=N), 144.4 (C_q), 143.8 (C_q), 135.9 (C_q), 134.4 (CH), 132.3 (CH), 132.2 (C_q), 130.7 (CH), 128.5 (C_q), 127.8 (CH), 127.2 (CH), 126.1 (CH), 125.1 (CH), 122.6 (CH), 115.6 (CH), 114.7 (CH), 113.1 (CH), 97.1 (C_{spiro}). **MS** (ESI) *m/z* calcd for $C_{21}H_{14}ClN_3O_2$: 375, found 376 [(^{35}Cl)M + H]$^+$; 378 [(^{37}Cl)M + H]$^+$. **HPLC purity** (ACN:H_2O, 70:30): retention time 6.25 min, 95%.

5-bromo-5'-(3-chlorophenyl)-3′-phenyl-3′H-spiro[indoline-3,2'- [1,3,4]**oxadiazol]-2-one 2:** Reaction time: 16 h. Yield: 61%, yellow solid, mp 225–227 °C. **IR** (NaCl, selected peaks) ν_{max} (cm^{-1}) 3282 (NH), 1743 (C=O), 1600 (C=N). **^{1}H-NMR** (300 MHz, Acetone-d_6) δ 10.10 (s, 1H, NH), 7.87–7.82 (m, 2H, ArH), 7.77 (t, J = 1.8 Hz, 1H, ArH), 7.70–7.67 (m, 1H, ArH), 7.58–7.53 (m, 2H, ArH), 7.24–7.13 (m, 3H, ArH), 6.94–6.86 (m, 3H, ArH). **^{13}C-NMR** (75 MHz, acetone-d_6) δ (ppm) 172.1 (C=O), 152.4 (C=N), 143.7 (C_q), 137.3 (CH), 136.0 (C_q), 132. (CH), 132.3 (CH), 130.9 (CH), 130.8 (CH), 128.5 (C_q), 127.5 (C_q), 127.4 (CH), 126.2 (CH), 122.9 (CH), 117.0 (C_q), 115.8 (CH), 115.1 (CH), 96.7 (C_{spiro}). **MS** (ESI) *m/z* calcd for $C_{21}H_{13}BrClN_3O_2$: 453, found 454 [(^{79}Br)(^{35}Cl)M + H]$^+$; 456 [(^{81}Br)(^{35}Cl)M + H]$^+$; 456 [(^{79}Br)(^{37}Cl)M + H]$^+$; 458 [(^{81}Br)(^{37}Cl)M + H]$^+$. **HPLC purity** (ACN:H_2O, 70:30): retention time 7.91 min, 97%.

5-chloro-5'-(3-chlorophenyl)-3′-phenyl-3′H-spiro[indoline-3,2'- [1,3,4]**oxadiazol]-2-one 3:** Reaction time: 16 h. Yield: 85%, yellow solid, mp > 300 °C. **IR** (NaCl, selected peaks) ν_{max} (cm^{-1}) 3283 (NH), 1726 (C=O), 1602 (C=N), 1570. **^{1}H-NMR** (300 MHz, Acetone-d_6) δ 9.80 (s, 1H, NH), 8.01–7.94 (m, 2H, ArH), 7.66–7.53 (m, 3H, ArH), 7.23–7.17 (m, 4H, ArH), 6.99–6.95 (m, 2H, ArH), 6.84–6.78 (m, 1H, ArH).**^{13}C NMR** (75 MHz, acetone-d_6) δ 172.2 (C=O), 152.4 (C=N), 143.7 (C_q), 143.2 (C_q), 136.0 (C_q), 134.4 (CH), 132.4 (CH), 132.3 (CH), 130.9 (CH), 129.9 (C_q), 128.5 (C_q), 128.0 (CH), 127.4 (CH), 127.1 (C_q), 126.2 (CH), 123.0 (CH), 115.8 (CH), 114.7 (CH), 96.8 (C_{spiro}). **MS** (ESI) *m/z* calcd for $C_{21}H_{13}Cl_2N_3O_2$: 409, found 410 [(^{35}Cl) M + H]$^+$; 412 [(^{35}Cl)(^{37}Cl) M + H]$^+$; 414 [(^{37}Cl) M + H]$^+$. **HPLC purity** (ACN:H_2O, 70:30): retention time 9.83 min, 96%.

7-chloro-5'-(3-chlorophenyl)-3′-phenyl-3′H-spiro[indoline-3,2'- [1,3,4]**oxadiazol]-2-one 4:** Reaction time: 16 h. Yield: 54%, yellow solid, mp 215–216 °C. **IR** (NaCl, selected peaks) ν_{max} (cm^{-1}) 3275 (NH), 1743 (C=O), 1597 (C=N). **^{1}H-NMR** (300 MHz, Acetone-d_6) δ 10.41 (s, 1H, NH), 7.88–7.83 (m, 2H, ArH), 7.59–7.54 (m, 4H, ArH), 7.24–7.17 (m, 3H, ArH), 6.94–6.86 (m, 3H, ArH). **^{13}C-NMR** (75 MHz, acetone-d_6) δ (ppm) 172.3 (C=O), 152.4 (C=N), 143.7 (C_q), 142.0 (C_q) 136.0 (C_q), 134.3 (CH), 132.4 (CH),132.3 (CH), 130.9 (CH),

128.4 (C_q), 127.4 (CH), 127.1 (C_q), 126.4 (CH1), 126.4 (CH2), 126.2 (CH), 123.0 (CH), 117.9 (C_q), 115.9 (CH), 97.3 (C_{spiro}). **MS** (ESI) *m/z* calcd for $C_{21}H_{13}Cl_2N_3O_2$: 409, found 410 [(^{35}Cl)M + H]$^+$; 412 [[(^{35}Cl)(^{37}Cl)M + H]$^+$; 414 [(^{37}Cl) M + H]$^+$. **HPLC purity** (ACN:H_2O, 70:30): retention time 8.17 min, 98%.

5-bromo-5'-(4-chlorophenyl)-3′-phenyl-3′H-spiro[indoline-3,2'- [1,3,4]**oxadiazol]-2-one 5:** Reaction time: 16 h. Yield: 51%, yellow solid, mp 123–125 °C. **IR** (NaCl, selected peaks) ν_{max} (cm^{-1}) 3275 (NH), 1743 (C=O), 1597 (C=N). **^{1}H-NMR** (300 MHz, acetone-d_6) δ (ppm) 10.14 (br s, 1H, NH), 7.93–7.88 (m, 2H, ArH), 7.77 (d, J = 2.1 Hz, 1H, ArH), 7.67 (dd, J = 8.3, 2.1 Hz, 1H, ArH), 7.56–7.50 (m, 2H, ArH), 7.23–7.13 (m, 3H, ArH), 6.97–6.78 (m, 3H, ArH). **^{13}C-NMR** (75 MHz, acetone-d_6) δ (ppm) 171.2 (C=O), 153.3 (C=N), 142.9 (C_q), 142.1 (C_q), 136.6 (CH), 132.0 (CH), 130.0 (CH1), 130.0 (CH2), 129.8 (CH), 127.2 (CH), 126.5 (C_q), 126.3 (C_q), 125.5 (C_q), 116.4 (CH), 116.3(C_q), 114.5 (CH), 95.7 (C_{spiro}); **MS** (ESI) *m/z* calcd for $C_{21}H_{13}BrClN_3O_2$: 453, found 454 [(^{79}Br)(^{35}Cl)M + H]$^+$; 456 [(^{81}Br)(^{35}Cl)M + H]$^+$; 456 [(^{79}Br)(^{37}Cl)M + H]$^+$; 458 [(^{81}Br)(^{37}Cl) M + H]$^+$. **HPLC purity** (ACN:H_2O, 70:30): retention time 8.32 min, 95%.

5-chloro-5'-(4-chlorophenyl)-3′-phenyl-3′H-spiro[indoline-3,2'- [1,3,4]**oxadiazol]-2-one 6:** Reaction time: 16 h. Yield: 68%, yellow solid, mp 123–125 °C. **IR** (NaCl, selected peaks) ν_{max} (cm^{-1}) 3275 (NH), 1743 (C=O), 1599 (C=N). **^{1}H-NMR** (300 MHz, Acetone-d_6) δ 10.14 (s, 1H, NH), 7.89 (d, J = 8.7 Hz, 2H, ArH), 7.65 (d, J = 2.1 Hz, 1H, ArH), 7.60–7.56 (m, 2H, ArH), 7.53 (d, J = 2.2 Hz, 1H, ArH), 7.23–7.17 (m, 3H, ArH), 6.97–6.84 (m, 3H, ArH). **^{13}C-NMR** (75 MHz, acetone-d_6) δ (ppm) 172.3 (C=O), 152.7 (C=N), 143.7 (C_q), 143.1 (C_q), 137.8 (C_q), 134.3 (CH), 130.9 (CH), 130.7 (CH), 129.9 (C_q), 129.4 (CH), 128.0 (CH), 127.1 (C_q), 125.3 (C_q), 122.8 (CH), 115.6 (CH), 114.7 (CH), 96.7 (C_{spiro}). **MS** (ESI) *m/z* calcd for $C_{21}H_{13}Cl_2N_3O_2$: 409, found 410 [(^{35}Cl)M + H]$^+$; 412 [(^{35}Cl)(^{37}Cl)M + H]$^+$; 414 [(^{37}Cl)M + H]$^+$. **HPLC purity** (ACN:H_2O, 70:30): retention time 7.12 min, 97%.

7-chloro-5'-(4-chlorophenyl)-3′-phenyl-3′H-spiro[indoline-3,2'- [1,3,4]**oxadiazol]-2-one 7:** Reaction time: 16 h. Yield: 67%, yellow solid, mp 229–231 °C. **IR** (NaCl, selected peaks) ν_{max} (cm^{-1}) 3227 (NH), 1747 (C=O), 1599 (C=N). **^{1}H-NMR** (300 MHz, Acetone-d_6) δ 10.44 (s, 1H, NH), 7.88 (d, J = 8.5 Hz, 2H, ArH), 7.59–7.51 (m, 4H, ArH), 7.22–7.16 (m, 3H, ArH), 6.91–6.84 (m, 3H, ArH). **^{13}C-NMR** (75 MHz, acetone-d_6) δ (ppm) 172.3 (C=O), 152.8 (C=N), 143.7 (C_q), 142.0 (C_q), 137.9 (C_q), 134.3 (CH), 130.9 (CH), 130.8 (CH), 129.4 (CH), 127.1 (C_q), 126.4 (CH), 125.2 (C_q), 122.9 (CH), 117.8 (C_q), 115.7 (CH), 97.2 (C_{spiro}). **MS** (ESI) *m/z* calcd for $C_{21}H_{13}Cl_2N_3O_2$: 409, found 410 [(^{35}Cl)M + H]$^+$; 412 [(^{35}Cl)(^{37}Cl)M + H]$^+$; 414 [(^{37}Cl)M + H]$^+$. **HPLC purity** (ACN:H_2O, 70:30): retention time 7.24 min, 99%.

5'-(4-methoxyphenyl)-3′-phenyl-3′H-spiro[indoline-3,2'- [1,3,4]**oxadiazol]-2-one 8**: Reaction time: 16 h. Yield: 42%, yellow solid, mp 224–226 °C. **IR** (NaCl, selected peaks) ν_{max} (cm^{-1}) 3419 (NH), 1743 (C=O), 1606 (C=N). **^{1}H NMR** (300 MHz, Acetone-d_6) δ 9.89 (s, 1H, NH), 7.86–7.82 (m, 2H, ArH), 7.54–7.47 (m, 2H, ArH), 7.18–7.02 (m, 6H, ArH), 6.91–6.87 (m, 3H, ArH), 3.89 (s, 3H, CH_3). **^{13}C-NMR** (75 MHz, acetone-d_6) δ 172.8 (C=O), 163.6 (C_q), 153.6 (C=N), 144.5 (C_q), 144.4 (C_q) 134.2 (CH), 130.6 (CH), 129.6 (CH), 127.7 (CH), 125.8 (C_q), 125.1 (CH), 122.1 (CH), 119.0 (CH), 115.9 (CH), 115.6 (C_q), 113.0 (CH), 96.6 (C_{spiro}), 56.7 (CH_3). **MS** (ESI) *m/z* calcd for $C_{22}H_{17}N_3O_3$: 371, found 372 [M+H]$^+$. **HPLC purity** (ACN:H_2O, 70:30): retention time 3.97 min, 100%.

5-bromo-5'-(4-methoxyphenyl)-3′-phenyl-3′H-spiro[indoline-3,2'- [1,3,4]**oxadiazol]-2-one 9:** Reaction time: 16 h. Yield: 62%, yellow solid, mp 164–166 °C. **IR** (NaCl, selected peaks) ν_{max} (cm^{-1}) 3275 (NH), 1743 (C=O), 1608 (C=N). **^{1}H-NMR** (300 MHz, Acetone-d_6) δ 9.57 (s, 1H, NH), 8.01–7.97 (m, 2H, ArH), 7.77 (dd, J = 8.4, 2.1 Hz, 1H, ArH), 7.69–7.68 (m, 1H, ArH), 7.21–7.14 (m, 2H, ArH), 7.07–7.03 (m, 3H, ArH), 6.96–6.93 (m, 2H, ArH), 6.81–6.76 (m, 1H, ArH), 3.89 (s, 3H, CH_3). **^{13}C-NMR** (75 MHz, acetone-d6) δ 184.3 (C=O), 167.8 (C_q), 164.2 (C_q), 160.0 (C_q), 151.6 (C=N), 151.2 (C_q), 142.0 (CH), 130.8 (CH), 130.4 (CH), 128.7 (CH), 127.1 (C_q), 121.3 (CH), 116.6 (C_q), 116.0 (CH), 115.3 (CH), 114.9 (CH), 96.7 (C_{spiro}), 56.6 (CH_3). **MS** (ESI) *m/z* calcd for $C_{22}H_{16}BrN_3O_3$: 449, found 450 [(^{79}Br) M + H]$^+$; 452 [(^{81}Br) M + H]$^+$. **HPLC purity** (ACN:H_2O, 70:30): retention time 6.34 min, 97%.

5-chloro-5'-(4-methoxyphenyl)-3′-phenyl-3′H-spiro[indoline-3,2'- [1,3,4]**oxadiazol]-2-one 10:** Reaction time: 16 h. Yield: 63%, yellow solid, mp 156–157 °C. **IR** (NaCl, selected peaks) ν_{max} (cm^{-1}) 3257 (NH), 1741 (C=O), 1593 (C=N). **^{1}H-NMR** (300 MHz, acetone-d_6) δ (ppm) 9.59 (s, 1H, NH), 7.99 (d, J = 8.8 Hz, 2H, ArH), 7.65–7.62 (m, 1H, ArH), 7.55 (s, 1H, ArH), 7.21–7.03 (m, 5H, ArH), 6.95 (d, J = 7.7 Hz, 2H, ArH), 6.76 (t, J = 7.3 Hz, 1H, ArH), 3.89 (s, 3H, CH_3). **^{13}C-NMR** (75 MHz, acetone-d_6) δ 184.7 (C=O), 167.7 (C_q), 164.2 (C_q), 151.6 (C=N), 150.9 (C_q), 139.1 (CH), 130.8 (CH), 130.4 (CH), 129.5 (C_q), 127.0 (C_q), 125.8 (CH), 121.2 (CH), 120.9 (C_q), 115.6 (CH), 115.3 (CH), 114.7 (CH), 96.6 (C_{spiro}), 56.6 (CH_3). **MS** (ESI) *m/z* calcd for $C_{22}H_{16}ClN_3O_3$: 405, found 406 [(^{35}Cl)M + H]$^+$; 408 [(^{37}Cl) M + H]$^+$.**HPLC purity** (ACN:H_2O, 70:30): retention time 5.68 min, 95%.

7-chloro-5'-(4-methoxyphenyl)-3′-phenyl-3′H-spiro[indoline-3,2'- [1,3,4]**oxadiazol]-2-one 11:** Reaction time: 16 h. Yield: 53%, yellow solid, mp 213–215 °C. **IR** (NaCl, selected peaks) ν_{max} (cm^{-1}) 3419 (NH), 1743 (C=O), 1604 (C=N). **^{1}H-NMR** (300 MHz, Acetone-d_6) δ 10.28 (s, 1H, NH), 7.86–7.81 (m, 2H, ArH), 7.69 (dd, J = 8.1, 1.1 Hz, 1H, ArH), 7.55 (td, J = 7.5, 3.1, 1.1 Hz, 1H, ArH), 7.49 (dd, J = 7.5, 1.1 Hz, 1H, ArH), 7.21–7.16 (m, 2H, ArH), 7.11–7.06 (m, 2H, ArH), 6.91–6.81 (m, 3H, ArH), 3.90 (s, 3H, CH_3). **^{13}C-NMR** (75 MHz, acetone-d_6) δ 173.0(C=O), 163.7 (C_q), 153.7 (C=N), 144.3 (C_q), 139.2 (CH), 134.1 (CH), 130.8 (CH), 129.6 (CH), 127.3 (C_q), 126.3 (CH), 125.7 (C_q), 124.7 (C_q), 122.5 (CH), 118.7 (C_q), 116.0 (CH), 115.7 (CH), 96.8 (C_{spiro}), 56.7 (CH_3). **MS** (ESI) *m/z* calcd for $C_{22}H_{16}ClN_3O_3$: 405, found 406 [(^{35}Cl)M + H]$^+$; 408 [(^{37}Cl)M + H]$^+$.**HPLC purity** (ACN:H_2O, 70:30): retention time 5.05 min, 98%.

3'-(3-chlorophenyl)-5′-phenyl-3′H-spiro[indoline-3,2'- [1,3,4]**oxadiazol]-2-one 12**: Reaction time: 16 h. Yield: 87%, yellow solid, mp 216–217 °C. **IR** (NaCl, selected peaks) ν_{max} (cm^{-1}) 3257 (NH), 1741 (C=O), 1593 (C=N). **^{1}H-NMR** (300 MHz, Acetone-d_6) δ 10.09 (s, 1H, NH), 7.91 (d, J = 5.0 Hz, 2H, ArH), 7.59–7.51 (m, 5H, ArH), 7.20–7.13 (m, 3H, ArH), 7.06 (s, 1H, ArH), 6.84 (d, J = 7.7 Hz, 1H, ArH), 6.64 (d, J = 7.8 Hz, 1H, ArH). **^{13}C-NMR** (75 MHz, acetone-d_6) δ (ppm) 171.4 (C=O), 153.4 (C=N), 144.4 (C_q), 143.6 (C_q), 135.4 (C_q), 133.9 (C_q), 132.0 (CH), 131.5 (CH), 129.8 (CH), 127.2 (CH), 127.1 (CH), 125.5 (C_q), 124.5 (CH), 123.7 (CH), 121.1 (CH), 114.6 (CH), 112.5 (CH), 112.4 (CH), 95.8 (C_{spiro}). **MS** (ESI) *m/z* calcd for $C_{21}H_{14}ClN_3O_2$: 375, found 376 [(^{35}Cl)M + H]$^+$; 378 [(^{37}Cl)M + H]$^+$.**HPLC purity** (ACN:H_2O, 70:30): retention time 6.00 min, 98%.

5-bromo-3'-(3-chlorophenyl)-5′-phenyl-3′H-spiro[indoline-3,2'- [1,3,4]**oxadiazol]-2-one 13:** Reaction time: 16 h. Yield: 64%, yellow solid, mp 222–223 °C. **IR** (NaCl, selected peaks) ν_{max} (cm^{-1}) 3254 (NH), 1743 (C=O), 1618, 1593 (C=N). **^{1}H-NMR** (300 MHz, Acetone-d_6) δ 10.23 (s, 1H, NH), 7.93–7.90 (m, 2H, ArH), 7.83 (d, J = 1.7 Hz, 1H, ArH), 7.72 (dd, J = 8.4, 2.1 Hz, 1H, ArH), 7.59–7.52 (m, 3H, ArH), 7.20–7.15 (m, 2H, ArH), 7.09 (t, J = 2.3 Hz, 1H, ArH), 6.88 (dd, J = 8.0, 1.1 Hz, 1H, ArH), 6.65 (dd, J = 8.2, 1.5 Hz, 1H, ArH). **^{13}C-NMR** (75 MHz, acetone-d_6) δ (ppm) 171.1 (C=O), 153.4 (C=N), 144.3 (C_q), 142.9 (C_q), 136.8 (CH), 135.5 (C_q), 132.1 (CH), 131.7 (CH), 130.1 (CH), 129.8 (CH), 127.3 (CH), 126.3 (C_q), 125.4 (C_q), 121.4 (CH), 116.5 (C_q), 114.8 (CH), 114.6 (CH), 112.4 (CH), 95.4 (C_{spiro}). **MS** (ESI) *m/z* calcd for $C_{21}H_{14}BrClN_3O_2$: 453, found 454 [(^{35}Cl)(^{79}Br)M + H]$^+$; 456 [(^{35}Cl)(^{81}Br)M + H]$^+$; 456 [(^{37}Cl)(^{79}Br)M + H]$^+$; 458 [(^{37}Cl)(^{81}Br)M + H]$^+$. **HPLC purity** (ACN:H_2O, 70:30): retention time 10.33 min, 96%.

5-chloro-3'-(3-chlorophenyl)-5′-phenyl-3′H-spiro[indoline-3,2'- [1,3,4]**oxadiazol]-2-one 14**: Reaction time: 16 h. Yield: 64%,

yellow solid, mp 209–210 °C. **IR** (NaCl, selected peaks) ν_{max} (cm-1) 3271 (NH), 1743 (C=O), 1593 (C=N). **^{1}H NMR** (300 MHz, Acetone-d_6) δ 10.16 (s, 1H, NH), 7.91 (dd, J = 7.7, 1.9 Hz, 2H, ArH), 7.68 (d, J = 2.1 Hz, 1H, ArH), 7.61–7.51 (m, 4H, ArH), 7.23–7.15 (m, 2H, ArH), 7.10 (t, J = 2.1 Hz, 1H, ArH), 6.89–6.86 (m, 1H, ArH), 6.68–6.64 (m, 1H, ArH). **^{13}C-NMR** (75 MHz, acetone-d_6) δ (ppm) 172.0 (C=O), 154.2 (C=N), 145.1 (C_q), 143.1 (C_q), 136.3 (C_q), 134.6 (CH), 132.8 (CH), 132.4 (CH), 130.5 (CH), 130.1 (C_q), 128.1 (CH), 128.0 (CH), 126.7 (C_q), 126.2 (C_q), 122.2 (CH), 115.6 (CH), 114.8 (CH), 113.3 (CH), 96.3 (C_{spiro}). **MS** (ESI) *m/z* calcd for $C_{21}H_{13}Cl_2N_3O_2$: 409, found 410 [(^{35}Cl)M + H]$^+$; 412 [(^{35}Cl)(^{37}Cl)M + H]$^+$; 414 [(^{37}Cl)M + H]$^+$. **HPLC purity** (ACN:H_2O, 70:30): retention time 9.30 min, 97%.

6-bromo-3'-(3-chlorophenyl)-5′-phenyl-3′H-spiro[indoline-3,2'- [1,3,4]**oxadiazol]-2-one 15***:* Reaction time: 15 h. Yield: 78%, yellow solid, mp 215–216 °C. **IR** (KBr, selected peaks) ν_{max} (cm^{-1}) 3265 (NH), 174.3 (C=O), 159.3 (C=N) cm^{-1}. **^{1}H-NMR** (300 MHz, acetone-d_6) δ (ppm) 10.16 (br s, 1H, NH), 7.92–7.89 (m, 2H, ArH), 7.57–7.50 (m, 4H, ArH), 7.37–7.34 (m, 2H, 2 ArH), 7.16 (t, J = 8.1 Hz, 1H, ArH), 7.09 (t, J = 2.1 Hz, 1H, ArH), 6.86 (ddd, J = 8.0, 2.0, 0.8 Hz, 1H, ArH), 6.63 (ddd, J = 8.3, 2.3, 0.8 Hz, 1H, ArH). **^{13}C-NMR** (75 MHz, acetone-d_6) δ (ppm) 171.3 (C=O), 153.5 (C=N), 145.1 (C_q), 144.4 (C_q), 135.5 (C_q), 132.1 (CH), 131.6 (CH), 129.8 (CH), 128.8 (CH), 127.5 (CH), 127.3 (CH), 127.1 (C_q), 125.4 (C_q), 123.3 (C_q), 121.5 (CH), 115.8 (CH), 115.0 (CH), 112.6 (CH), 95.5 (C_{spiro}). **Anal.** Calcd. for $C_{21}H_{13}BrClN_3O_2$: C 55.47%, H 2.88%, N 9.24%, found: C 54.94%, H 3.39%, N 9.12%.

6-chloro-3'-(3-chlorophenyl)-5′-phenyl-3′H-spiro[indoline-3,2'- [1,3,4]**oxadiazol]-2-one 16:** Reaction time: 15 h. Yield: 43%, yellow solid, mp 224–225 °C. **IR** (KBr, selected peaks) ν_{max} (cm^{-1}) 3140 (NH), 1740 (C=O), 1616 (C=N) cm^{-1}. **^{1}H-NMR** (300 MHz, acetone-d_6) δ (ppm) 10.16 (br s, 1H, NH), 7.92–7.89 (m, 2H, ArH), 7.60–7.53 (m, 4H, ArH), 7.21–7.13 (m, 3H, ArH), 7.09 (t, J = 2.1 Hz, 1H, ArH), 6.86 (ddd, J = 8.0, 2.0, 0.8 Hz, 1H, ArH), 6.63 (ddd, J = 8.3, 2.3, 0.8 Hz, 1H, ArH). **^{13}C-NMR** (75 MHz, acetone-d_6) δ (ppm) 171.4 (C=O), 153.5 (C=N), 145.0 (C_q), 144.4 (C_q), 139.0 (C_q), 135.5 (C_q), 132.1 (CH), 131.6 (CH), 129.8 (CH), 128.6 (CH), 127.2 (CH), 125.4 (C_q), 124.5 (CH), 122.8 (C_q), 121.5 (CH), 115.0 (CH), 113.0 (CH), 112.6 (CH), 95.4 (C_{spiro}). **Anal.** Calcd. for $C_{21}H_{13}Cl_2N_3O_2$: C 61.48%, H 3.19%, N 10.24%, Found: C 61.31%, H 3.58%, N 10.13%.

7-chloro-3'-(3-chlorophenyl)-5′-phenyl-3′H-spiro[indoline-3,2'- [1,3,4]**oxadiazol]-2-one 17:** Reaction time: 16 h. Yield: 68%, yellow solid, mp 205–207 °C. **IR** (NaCl, selected peaks) ν_{max} (cm^{-1}) 3381 (NH), 1747 (C=O), 1595 (C=N). **^{1}H NMR** (300 MHz, Acetone-d_6) δ 10.43 (s, 1H, NH), 7.94–7.91 (m, 2H, ArH), 7.62–7.52 (m, 5H, ArH), 7.24–7.15 (m, 2H, ArH), 7.11 (t, J = 2.1 Hz, 1H, ArH), 6.88 (dd, J = 7.9, 1.9 Hz, 1H, ArH), 6.63 (dd, J = 8.3, 1.5 Hz, 1H, ArH). **^{13}C NMR** (75 MHz, acetone-d_6) δ (ppm) 172.0 (C=O), 154.3 (C=N), 145.1 (C_q), 136.3 (C_q), 134.5 (CH), 132.9 (CH), 132.4 (CH), 130.6 (CH), 128.0 (CH), 126.7 (C_q), 126.5 (CH1), 126.5 (CH2), 126.1 (C_q), 122.3 (CH), 118.0 (C_q), 115.8 (CH), 113.4 (CH), 96.8 (C_{spiro}). **MS** (ESI) *m/z* calcd for $C_{21}H_{13}Cl_2N_3O_2$: 409, found 410 [(^{35}Cl)M + H]$^+$; 412 [(^{35}Cl)(^{37}Cl)M + H]$^+$; 414 [(^{37}Cl)M + H]$^+$. **HPLC purity** (ACN:H_2O, 70:30): retention time 7.70 min, 97%.

5-bromo-3'-(4-chlorophenyl)-5′-phenyl-3′H-spiro[indoline-3,2'- [1,3,4]**oxadiazol]-2-one 18:** Reaction time: 15 h. Yield: 74%, yellow solid, mp 216–217 °C. **IR** (KBr, selected peaks) ν_{max} (cm^{-1}) 3462 (NH), 1762 (C=O), 1616 (C=N) cm^{-1}. **^{1}H-NMR** (300 MHz, acetone-d_6) δ (ppm) 10.19 (br s, 1H, NH), 7.90–7.87 (m, 2H, ArH), 7.79 (d, J = 2.0 Hz, 1H, ArH), 7.69 (dd, J = 8.4, 2.1 Hz, 1H, ArH), 7.57–7.51 (m, 3H, ArH), 7.24–7.19 (m, 2H, ArH), 7.13 (d, J = 8.4 Hz, 1H, ArH), 6.92–6.89 (m, 2H, ArH). **^{13}C-NMR** (75 MHz, acetone-d_6) δ (ppm) 171.1 (C=O), 153.2 (C=N), 142.9 (C_q), 142.0 (C_q), 136.6 (CH), 131.9 (CH), 130.0 (CH1), 130.0 (CH2), 129.7 (CH), 127.2 (CH), 126.4 (C_q), 126.2 (C_q), 125.5 (C_q), 116.3 (CH), 115.4 (C_q), 114.5 (CH), 95.6 (C_{spiro}). **MS** (ESI) *m/z* calcd for $C_{21}H_{13}BrClN_3O_2$: 453, found 454 [(^{35}Cl)(^{79}Br)M + H]$^+$; 456 [(^{35}Cl)(^{81}Br)M + H]$^+$; 456 [(^{37}Cl)(^{79}Br)M + H]$^+$; 458 [(^{37}Cl)(^{81}Br)M + H]$^+$. **Anal.** Calcd. ($C_{21}H_{13}BrClN_3O_2$): C, 55.47%; H, 2.88%; N, 9.24%, found C, 55.64%; H, 3.14%; N, 8.87%.

7-chloro-3'-(4-chlorophenyl)-5′-phenyl-3′H-spiro[indoline-3,2'- [1,3,4]**oxadiazol]-2-one 19**: Reaction time: 16 h. Yield: 68%, yellow solid, mp130 − 131 °C. **IR** (NaCl, selected peaks) ν_{max} (cm^{-1}) 3273 (NH), 1745 (C=O), 1599 (C=N). **^{1}H-NMR** (300 MHz, acetone-d_6) δ (ppm) 10.41 (s, 1H, NH), 7.92–7.89 (m, 2H, ArH), 7.60–7.52 (m, 5H, ArH), 7.26–7.18 (m, 3H, ArH), 6.94–6.89 (m, 2H, ArH). **^{13}C-NMR** (75 MHz, acetone-d_6) δ (ppm) 172.1 (C=O), 154.1 (C=N), 142.9 (C_q), 142.0 (C_q), 134.4 (CH), 132.8 (CH), 130.8 (CH), 130.6 (CH), 127.9 (CH), 127.1 (C_q), 126.8 (C_q), 126.4 (CH1), 126.4 (CH2), 126.2 (C_q), 118.0 (C_q), 117.3 (CH), 97.0 (C_{spiro}). **MS** (ESI) *m/z* calcd for $C_{21}H_{13}Cl_2N_3O_2$: 409, found 410 [(^{35}Cl)M + H]$^+$; 412 [(^{35}Cl)(^{37}Cl)M + H]$^+$; 414 [(^{37}Cl)M + H]$^+$. **HPLC purity** (ACN:H_2O, 70:30): retention time 7.33 min, 99%.

7-chloro-3′,5′-bis(3-chlorophenyl)-3′H-spiro[indoline-3,2'- [1,3,4]**oxadiazol]-2-one 20**: Reaction time: 16 h. Yield: 67%, yellow solid, mp 219–220 °C. **IR** (NaCl, selected peaks) ν_{max} (cm^{-1}) 3225 (NH), 1747 (C=O), 1595 (C=N). **^{1}H-NMR** (300 MHz, acetone-d_6) δ (ppm) 10.45 (s, 1H, NH), 7.92–7.86 (m, 2H, ArH), 7.62–7.55 (m, 4H, ArH), 7.25–7.17 (m, 2H, ArH), 7.13 (t, J = 2.1 Hz, 1H, ArH), 6.93–6.87 (m, 1H, ArH), 6.63 (dd, J = 8.3, 2.2 Hz, 1H, ArH). **^{13}C-NMR** (75 MHz, acetone-d_6) δ (ppm) 171.8 (C=O), 153.0 (C=N), 144.8 (C_q), 136.3 (C_q), 134.6 (C_q), 134.2 (C_q), 132.7 (CH), 132.5 (CH), 130.8 (C_q), 130.5 (CH), 127.8 (CH), 127.6 (CH), 126.6 (CH), 126.4 (CH), 122.7 (C_q), 122.6 (CH), 118.0 (C_q), 115.8 (CH). 115.7 (CH), 113.4 (CH), 97.1 (C_{spiro}). **MS** (ESI) *m/z* calcd for $C_{21}H_{12}Cl_3N_3O_2$: 443, found 444 [(^{35}Cl)M + H]$^+$; 446 [(^{35}Cl)(^{35}Cl)(^{37}Cl)M + H]$^+$; 448 [(^{35}Cl)(^{37}Cl)(^{37}Cl)M + H]$^+$; 450 [(^{37}Cl)M + H]$^+$. **HPLC purity** (ACN:H_2O, 70:30): retention time 5.49 min, 98%.

5-bromo-5'-(*tert*-butyl)-3'-(2-chlorophenyl)-3′H-spiro[indoline-3,2'- [1,3,4]**oxadiazol]-2-one 21:** Reaction time: 15 h. Yield: 65%, dark yellow solid, mp 213–214. **IR** (KBr, selected peaks) ν_{max} (cm^{-1}) 3298 (NH), 2968 (C–H), 1716 (C=O), 1618 (C=N). **^{1}H-NMR** (300 MHz, acetone-d_6) δ (ppm) 9.72 (br s, 1H, NH), 7.60 (dd, J = 8.1, 1.5 Hz, 1H, ArH), 7.45 (dd, J = 8.3, 2.1 Hz, 1H, ArH), 7.36–7.30 (m, 1H, ArH), 7.18 (dd, J = 8.0, 1.5 Hz, 1H, ArH), 7.12–7.06 (m, 1H, ArH), 6.91 (d, J = 8.4 Hz, 1H, ArH), 6.88 (d, J = 2.0 Hz, 1H, ArH), 1.37 (s, 9H, $C(CH_3)_3$). **^{13}C-NMR** (75 MHz, acetone-d_6) δ (ppm) 171.3 (C=O), 165.3 (C=N), 143.0 (C_q), 142.7 (C_q), 134.8 (CH), 129.5 (CH), 129.4 (CH), 127.7 (C_q), 127.3 (CH), 126.1 (CH), 124.9 (CH), 124.7 (C_q), 113.6 (C_q), 112.7 (CH), 95.8 (C_{spiro}), 32.0 ($\underline{C}(CH_3)_3$), 26.8 ($C(\underline{C}H_3)_3$). **Anal.** Calcd. for $C_{19}H_{17}BrClN_3O_2$: C 52.50%, H 3.94%, N 9.67%, found: C 52.53%, H 4.29%, N 9.53%.

5'-(*tert*-butyl)-5-chloro-3'-(2-chlorophenyl)-3′H-spiro[indoline-3,2'- [1,3,4]**oxadiazol]-2-one 22**: Reaction time: 15 h. Yield: 65%, white solid, mp 219–220 °C. **IR** (KBr, selected peaks) ν_{max} (cm^{-1}) 3291 (NH), 2968 (C–H), 1761 (C=O), 1654 (C=N). **^{1}H-NMR** (300 MHz, acetone-d_6) δ (ppm) 9.63 (br, s, 1H, NH), 7.59 (dd, J = 8.1, 1.5 Hz, 1H, ArH), 7.35–7.29 (m, 2H, ArH), 7.17 (dd, J = 8.0, 1.5 Hz, 1H, ArH), 7.11–7.05 (m, 1H, ArH), 6.95 (d, J = 8.4 Hz, 1H, ArH), 6.77 (d, J = 2.2 Hz, 1H, ArH), 1.37 (s, 9H, $C(CH_3)_3$). **^{13}C-NMR** (75 MHz, acetone-d_6) δ (ppm) 172.2 (C=O), 166.1 (C=N), 143.5 (C_q), 143.4 (C_q), 132.7 (CH), 130.3 (CH), 128.6 (C_q), 128.1 (CH), 127.8 (C_q), 127.4 (CH), 126.9 (CH), 125.8 (CH), 125.3 (C_q), 113.0 (CH), 96.7 (C_{spiro}), 32.8 ($\underline{C}(CH_3)_3$), 27.7 ($C(\underline{C}H_3)_3$). **Anal.** Calcd. for $C_{19}H_{17}Cl_2N_3O_2$: C 58.48%, H 4.39%, N 10.77%, found: C 58.15%, H 4.47%, N 10.60%.

5-bromo-5'-(*tert*-butyl)-3'-(3-chlorophenyl)-3′H-spiro[indoline-3,2'- [1,3,4]**oxadiazol]-2-one 23**: Reaction time: 15 h. Yield: 70%, white solid, mp 221–222 °C. **IR** (KBr, selected peaks) ν_{max} (cm^{-1}) 3292 (NH), 2976 (C–H), 1765 (C=O), 1616 (C=N). **^{1}H-NMR** (300 MHz, acetone-d_6) δ (ppm) 10.13 (br s, 1H, NH), 7.68–7.64 (m, 2H, ArH), 7.13–7.08 (m, 2H, ArH), 6.93 (t, J = 2.1 Hz, 1H, ArH), 6.80 (ddd, J = 7.9, 2.0, 0.8 Hz, 1H, ArH), 6.49 (ddd, J = 8.3, 2.2, 0.8 Hz, 1H,

ArH), 1.33 (s, 9H, C(CH_3)$_3$). **^{13}C NMR** (75 MHz, acetone-d_6) δ (ppm) 171.2 (C═O), 162.5 (C═N), 144.9 (C_q), 142.7 (C_q), 136.4 (CH), 135.3 (C_q), 131.4 (CH), 129.6 (CH), 126.7 (C_q), 120.9 (CH), 116.2 (C_q), 114.5 (CH), 114.3 (CH), 112.2 (CH), 95.1 (C_{spiro}), 32.7 (C(CH_3)$_3$), 27.5 (C(CH_3)$_3$). **MS** (ESI) *m/z* calcd for $C_{19}H_{17}BrClN_3O_2$: 433, found 434 [(^{35}Cl)(^{79}Br)M + H]$^+$; 436 [(^{35}Cl)(^{81}Br)M + H]$^+$; 436 [(^{37}Cl)(^{79}Br)M + H]$^+$; 438 [(^{37}Cl)(^{81}Br)M + H]$^+$.**HPLC purity** (ACN:H_2O, 70:30): retention time 9.42 min, 97%.

5'-(*tert*-butyl)-5-chloro-3'-(3-chlorophenyl)-3′H-spiro[indoline-3,2'- [1,3,4]**oxadiazol]-2-one 24**: Reaction time: 15 h. Yield: 64%, yellow solid, mp 229–230 °C. **IR** (KBr, selected peaks) ν_{max} (cm^{-1}) 3286 (NH), 2978 (C–H), 1765 (C═O), 1616 (C═N). **^{1}H-NMR** (300 MHz, acetone-d_6) δ (ppm) 10.03 (br s, 1H, NH), 7.54–7.51 (m, 2H, ArH), 7.17–7.08 (m, 2H, H, ArH), 6.93 (t, J = 2.1 Hz, 1H, ArH), 6.81 (ddd, J = 8.0, 2.0, 0.8 Hz, 1H, ArH), 6.52 (ddd, J = 8.3, 2.3, 0.8 Hz, 1H, ArH), 1.35 (s, 9H, C(CH_3)$_3$). **^{13}C-NMR** (75 MHz, acetone-d_6) δ (ppm) 171.4 (C═O), 162.6 (C═N), 145.0 (C_q), 142.3 (C_q), 135.3 (C_q), 133.5 (CH), 131.4 (CH), 129.2 (C_q), 126.8 (C_q), 126.5 (CH), 120.9 (CH), 114.7 (CH), 113.9 (CH), 112.4 (CH), 95.3 (C_{spiro}), 32.7 (C(CH_3)$_3$), 27.5 (C(CH_3)$_3$). **Anal.** Calcd. For $C_{19}H_{17}Cl_2N_3O_2$**:** C 58.48%, H 4.39%, N 10.77%, found: C 58.12%, H 4.60%, N 10.60%.

6-bromo-5'-(*tert*-butyl)-3'-(3-chlorophenyl)-3′H-spiro[indoline-3,2'- [1,3,4]**oxadiazol]-2-one 25**: Reaction time: 15 h. Yield: 53%, yellow solid, mp 213–214 °C. **IR** (KBr, selected peaks) ν_{max} (cm^{-1}) 3155 (NH), 2974 (C–H), 1744 (C═O), 1616 (C═N). **^{1}H-NMR** (300 MHz, acetone-d_6) δ (ppm) 10.03 (br s, 1H, NH), 7.40–7.37 (m, 1H, ArH), 7.34–7.33 (m, 1H, ArH), 7.31–7.30 (m, 1H, ArH), 7.10 (t, J = 8.1 Hz, 1H, ArH), 6.94 (t, J = 2.1 Hz, 1H, ArH), 6.79 (ddd, J = 8.0, 2.0, 0.9 Hz, 1H, ArH), 6.50 (ddd, J = 8.3, 2.3, 0.9 Hz, 1H, ArH), 1.33 (s, 9H, C(CH_3)$_3$). **^{13}C-NMR** (75 MHz, acetone-d_6) δ (ppm) 171.5 (C═O), 162.6 (C═N), 145.1 (C_q), 144.9 (C_q), 135.3 (C_q), 131.4 (CH), 128.3 (CH), 127.4 (CH), 126.7 (C_q), 123.7 (C_q), 120.9 (CH), 115.6 (CH), 114.7 (CH), 112.4 (CH), 95.2 (C_{spiro}), 32.7 (C(CH_3)$_3$), 27.5 (C(CH_3)$_3$). **Anal.** Calcd. For $C_{19}H_{17}BrClN_3O_2$: C 52.50%, H 3.94%, N 9.67%, Found: C 52.75%, H 4.29%, N 9.47%.

5'-(*tert*-butyl)-6-chloro-3'-(3-chlorophenyl)-3′H-spiro[indoline-3,2'- [1,3,4]**oxadiazol]-2-one 26**: Reaction time: 15 h. Yield: 80%, white solid, mp 209–211 °C. **IR** (KBr, selected peaks) ν_{max} (cm^{-1}) 3155 (NH), 2972 (C–H), 1744 (C═O), 1620 (C═N). **^{1}H-NMR** (300 MHz, acetone-d_6) δ (ppm) 10.13 (br, s, 1H, NH), 7.47–7.45 (m, 1H, ArH), 7.18–7.15 (m, 2H, ArH), 7.10 (t, J = 8.1 Hz, 1H, ArH), 6.94 (t, J = 2.1 Hz, 1H, ArH), 6.79 (ddd, J = 7.9, 1.9, 0.8 Hz, 1H, ArH), 6.49 (ddd, J = 8.3, 2.2, 0.7 Hz, 1H, ArH), 1.32 (s, 9H, C(CH_3)$_3$). **^{13}C-NMR** (75 MHz, acetone-d_6) δ (ppm) 171.6 (C═O), 162.5 (C═N), 145.0 (C_q), 144.8 (C_q), 138.6 (C_q), 135.3 (C_q), 131.4 (CH), 128.1 (CH), 124.3 (CH), 123.2 (C_q), 120.8 (CH), 114.6 (CH), 112.8 (CH), 112.3 (CH), 95.0 (C_{spiro}), 32.6 (C(CH_3)$_3$), 27.4 (C(CH_3)$_3$). **Anal.** Calcd. For $C_{19}H_{17}Cl_2N_3O_2$: C 58.48%, H 4.39%, N 10.77%, Found: C 58.04%, H 4.78%, N 10.43%.

4.2. Activity against erythrocyte-stage P. falciparum

These experiments were performed according to a previously described method [43]. Briefly, human erythrocytes infected with 1% ring-stage W2-strain *P. falciparum* synchronized with 5% sorbitol were incubated with test compounds in 96-well plates at 37 °C for 48 h in RPMI-1640 medium, supplemented with 25 mM 4-(2-hydroxyethyl)-1-piperazineethanesulfonic acid (HEPES) pH 7.4, 10% heat inactivated human serum (or 0.5% Albumax, 2% human serum), and 100 μM hypoxanthine under an atmosphere of 3% O_2, 5% CO_2, and 91% N_2. After 48 h, the cells were fixed in 2% formaldehyde in phosphate-buffered saline (PBS) and transferred into PBS with 100 mM NH_4Cl, 0.1% Triton X-100, 1 nM YOYO-1, and infected erythrocytes were counted in a flow cytometer (FACSort, Beckton Dickinson; EX 488 nm, EM 520 nm). IC_{50}s based on comparisons with untreated control cultures were calculated with GraphPad PRISM software. Two independent experiments were performed, each with four replicates for each of the experimental conditions.

4.3. Activity against hepatic P. berghei infection

The *in vitro* inhibition of hepatocyte infection by *P. berghei* was determined by measuring the luminescence intensity of Huh-7 cells infected with a firefly-luciferase-expressing *P. berghei* line (PbGFP-Luccon), as previously described [44,45]. Huh7 cells, a human hepatoma cell line, were cultured in RPMI-1640 medium supplemented with 10% fetal calf serum (FCS), 1% v/v penicillin/streptomycin, 1% v/v glutamine, 1% v/v non-essential amino acids and 10 mM HEPES pH 7 (cRPMI), and incubated at 37 °C, 5% CO_2. For the infection assay, the cells were seeded at 1 × 10^4 cells/well of a 96-well plate in cRPMI, and incubated at 37 °C, 5% CO_2. Stock solutions of 10 mM of each compound were prepared by dissolving the accurately weighed compounds in DMSO and stored at −20 °C. On the day of drug treatment and infection, approximately 1 h prior to infection, the medium was replaced by medium containing the appropriate concentration of each compound, diluted in cRPMI medium further supplemented with gentamicin (50 μg/mL) and amphotericin B (0.8 μg/mL). As a control, a dilution of DMSO that mimics the highest concentration of compound used was employed. Sporozoites freshly obtained through the disruption of the salivary glands of infected female *Anopheles stephensi* mosquitoes were added 1 h after compound addition to the cells at a proportion of 1:1 (1 × 10^4 sporozoites/well). The sporozoite addition was followed by centrifugation at 1800×*g* for 5 min, and incubation for 46 h at 37 °C, 5% CO_2. The assessment of compound activity was determined by measuring cell-confluency, using the AlamarBlue assay, according to the manufacturer's instructions. Briefly, AlamarBlue diluted 1:20 in cRPMI, was added to the cells and incubated for 90 min at 37 °C, 5% CO_2, before measuring fluorescence and determining cell-viability. Finally, 48 h post-infection, drug activity was assessed by measuring luminescence of infected Huh-7 cell lysates, following the addition of the luciferin substrate. Nonlinear regression analysis was employed to fit the normalized results of the dose-response curves, and IC_{50} values were determined using the GraphPad Prism software.

4.4. Measurements of cytosolic Na^+ concentration in P. falciparum

Mature trophozoite-stage parasites (3D7 strain) were isolated from their host erythrocytes via brief exposure to saponin and loaded with the Na^+-sensitive dye SBFI, as described previously [16]. Measurements were performed in a Tecan fluorescence spectrometer plate-reader with parasites suspended at 37 °C in a pH 7.1 physiological saline solution containing 125 mM NaCl, 5 mM KCl, 1 mM $MgCl_2$, 20 mM glucose and 25 mM HEPES. The excitation wavelengths were 340 nm and 380 nm, with emission recorded at 515 nm. The ratio of the fluorescence intensity at 340 nm and 380 nm was converted to $[Na^+]_{cyt}$ using a previously described calibration procedure [16].

4.5. Membrane preparation and ATPase assays

Membranes were prepared from saponin-isolated *P. falciparum* parasites (3D7 strain) using a previously described method [36]. A PiColorLock Phosphate Assay Kit (Abcam) was used to quantify the production of P_i from the hydrolysis of ATP. The reactions were performed at 37 °C, and the reaction mixtures had a pH of 7.2 and contained 20 mM KCl, 2 mM $MgCl_2$, 50 mM Tris, and either 150 mM NaCl or 150 mM choline chloride. Parasite membrane was added to give a final concentration of total protein of 50 μg/mL. ATP (1 mM

$Na_2ATP.3H_2O$; MP Biomedicals) was added last to commence the reaction, introducing 2 mM Na^+ to each reaction. The DMSO concentration in the reactions did not exceed 0.3% v/v. The reactions were terminated after 10 min by transferring aliquots (100 μL) of the reaction mixture in duplicate into wells of a 96 well plate containing 25 μL of PiColorLock with 1% v/v Accelerator. Stabilizer (10 μL) was added to the wells 3 min later and the plates were incubated at room temperature for 1 h before absorbance was measured at 635 nm. Control values, from wells in which all components were present but to which ATP was not added until after the exposure of membrane to PiColorLock, were subtracted from the data.

4.6. In silico study of chemical similarity

The library of known antimalarials in clinical and preclinical phases was downloaded from the DrugBank database [34]. For each compound, the protonation state was assigned by QUACPAC (OpenEye Scientific Software Santa Fe, version 2.0.2.2), while energy minimization was performed with Szybki version 1.11.0.2 (OpenEye Scientific Software, Santa Fe, NM) using the MMFF94S force field [46–48]. A conformational database containing up to 600 conformers of each spirooxadiazoline oxindole compound was generated by conformational analysis with OMEGA version 3.1.2.2 (OpenEye Scientific Software, Santa Fe, NM) [49,50]. These conformers were screened against each ROCS query using the ROCS program version 3.3.0.3 (OpenEye Scientific Software, Santa Fe, NM) [51]. Results were ranked based on the Tanimoto Combo score.

Declaration of competing interest

The authors declare that they have no known competing financial interests or personal relationships that could have appeared to influence the work reported in this paper.

Acknowledgments

This work was supported by FCT (Fundação para a Ciência e a Tecnologia, I.P.) through iMed.ULisboa (UID/DTP/04138/2019), project PTDC/QUI-QOR/29664/2017, and PhD fellowship SFRH/BD/137544/2018 (E. Lopes). The NMR spectrometers are part of the National NMR Network (PTNMR) and are partially supported by Infrastructure Project Nº 022161 (co-financed by FEDER through COMPETE 2020, POCI and PORL and FCT through PIDDAC). Financial support from FCT and Portugal 2020 to the Portuguese Mass Spectrometry Network (Rede Nacional de Espectrometria de Massa – RNEM; LISBOA-01-0145-FEDER-402-022125) is also acknowledged. We wish to thank the OpenEye Free Academic Licensing Programme for providing a free academic licence for molecular modeling and chemoinformatics software. We are grateful to Julia Lindblom for performing an initial Na^+ assay with **18** at 5 μM, and to Australian Red Cross Lifeblood for the provision of blood for parasite culture.

Appendix A. Supplementary data

Supplementary data to this article can be found online at https://doi.org/10.1016/j.ejmech.2022.114324.

References

[1] WHO, World Malaria Report 2021, WHO, 2021. https://www.mmv.org/sites/default/files/uploads/docs/publications/World_Malaria_Report_2021.pdf. (Accessed 28 April 2022).
[2] T. Rodrigues, M. Prudêncio, R. Moreira, M.M. Mota, F. Lopes, Targeting the liver stage of malaria parasites: a yet Unmet Goal, J. Med. Chem. 55 (2012) 995–1012, https://doi.org/10.1021/jm201095h.
[3] S.H. Shafik, S.A. Cobbold, K. Barkat, S.N. Richards, N.S. Lancaster, M. Llinás, S.J. Hogg, R.L. Summers, M.J. McConville, R.E. Martin, The natural function of the malaria parasite's chloroquine resistance transporter, Nat. Commun. 11 (2020) 3922, https://doi.org/10.1038/s41467-020-17781-6.
[4] WHO, Guidelines for the Treatment of Malaria, third ed., World Health Organization, 2015.
[5] Identifier NCT01054248, Randomised trial of 3 artemisinin combination therapy for malaria in pregnancy (DMA), in: ClinicalTrials.gov, National Library of Medicine (US), Bethesda (MD), 2010 Feb 16.
[6] Identifier NCT02297477, The ASAP study - therapeutic efficacy of Atovaquone-proguanil vs. Artesunate-atovaquone-proguanil in Cambodia (ASAP), in: ClinicalTrials.gov, National Library of Medicine (US), Bethesda (MD), 2014 Dec.
[7] E.A. Lopes, M.M.M. Santos, M. Mori, Pharmacological treatment of malaria, in: C. Supuran (Ed.), Antiprotozoan Drugs, Springer, 2021.
[8] P.G. Mathenge, S.K. Low, N.L. Vuong, M.Y.F. Mohamed, H.A. Faraj, G.I. Alieldin, R. Al khudari, N.A. Yahia, A. Khan, O.M. Diab, Y.M. Mohamed, A.H. Zayan, G.M. Tawfik, N.T. Huy, K. Hirayama, Efficacy and resistance of different artemisinin-based combination therapies: a systematic review and network meta-analysis, Parasitol. Int. 74 (2020) 101919, https://doi.org/10.1016/j.parint.2019.04.016.
[9] C. Nsanzabana, Resistance to artemisinin combination therapies (ACTs): do not forget the partner drug, Tropical Med. Infect. Dis. 4 (2019) 26, https://doi.org/10.3390/tropicalmed4010026.
[10] G. Camarda, P. Jirawatcharadech, R.S. Priestley, A. Saif, S. March, M.H.L. Wong, S. Leung, A.B. Miller, D.A. Baker, P. Alano, M.J.I. Paine, S.N. Bhatia, P.M. O'Neill, S.A. Ward, G.A. Biagini, Antimalarial activity of primaquine operates via a two-step biochemical relay, Nat. Commun. 10 (2019) 3226, https://doi.org/10.1038/s41467-019-11239-0.
[11] E.R. Derbyshire, M.M. Mota, J. Clardy, The next opportunity in anti-malaria drug discovery: the liver stage, PLoS Pathog. 7 (2011), e1002178, https://doi.org/10.1371/journal.ppat.1002178.
[12] M. De Rycker, B. Baragaña, S.L. Duce, I.H. Gilbert, Challenges and recent progress in drug discovery for tropical diseases, Nature 559 (2018) 498–506, https://doi.org/10.1038/s41586-018-0327-4.
[13] T.M. Belete, Recent progress in the development of new antimalarial drugs with novel targets, Drug Des. Dev. Ther. 14 (2020) 3875–3889, https://doi.org/10.2147/DDDT.S265602.
[14] B.K.S. Yeung, B. Zou, M. Rottmann, S.B. Lakshminarayana, S.H. Ang, S.Y. Leong, J. Tan, J. Wong, S. Keller-Maerki, C. Fischli, A. Goh, E.K. Schmitt, P. Krastel, E. Francotte, K. Kuhen, D. Plouffe, K. Henson, T. Wagner, E.A. Winzeler, F. Petersen, R. Brun, V. Dartois, T.T. Diagana, T.H. Keller, Spirotetrahydro β-Carbolines (spiroindolones): a new class of potent and orally efficacious compounds for the treatment of malaria, J. Med. Chem. 53 (2010) 5155–5164, https://doi.org/10.1021/jm100410f.
[15] M. Rottmann, C. McNamara, B.K.S. Yeung, M.C.S. Lee, B. Zou, B. Russell, P. Seitz, D.M. Plouffe, N.V. Dharia, J. Tan, S.B. Cohen, K.R. Spencer, G.E. González-Páez, S.B. Lakshminarayana, A. Goh, R. Suwanarusk, T. Jegla, E.K. Schmitt, H.-P. Beck, R. Brun, F. Nosten, L. Renia, V. Dartois, T.H. Keller, D.A. Fidock, E.A. Winzeler, T.T. Diagana, Spiroindolones, a potent compound class for the treatment of malaria, Science 329 (2010) 1175–1180, https://doi.org/10.1126/science.1193225.
[16] N.J. Spillman, R.J.W. Allen, C.W. McNamara, B.K.S. Yeung, E.A. Winzeler, T.T. Diagana, K. Kirk, Na^+ regulation in the malaria parasite Plasmodium falciparum involves the cation ATPase *Pf*ATP4 and is a target of the spiroindolone antimalarials, Cell Host Microbe 13 (2013) 227–237, https://doi.org/10.1016/j.chom.2012.12.006.
[17] C.J.A. Ribeiro, J.D. Amaral, C.M.P. Rodrigues, R. Moreira, M.M.M. Santos, Spirooxadiazoline oxindoles with promising in vitro antitumor activities, Med. Chem. Comm. 7 (2016) 420–425, https://doi.org/10.1039/C5MD00450K.
[18] C.J.A. Ribeiro, R.C. Nunes, J.D. Amaral, L.M. Gonçalves, C.M.P. Rodrigues, R. Moreira, M.M.M. Santos, Spirotriazoline oxindoles: a novel chemical scaffold with in vitro anticancer properties, Eur. J. Med. Chem. 140 (2017) 494–509, https://doi.org/10.1016/j.ejmech.2017.09.037.
[19] J.D. Amaral, D. Silva, C.M.P. Rodrigues, S. Solá, M.M.M. Santos, A novel small molecule p53 stabilizer for brain cell differentiation, Front. Chem. 7 (2019), https://doi.org/10.3389/fchem.2019.00015.
[20] T.P. Singh, O.M. Singh, Recent progress in biological activities of indole and indole Alkaloids, Mini Rev. Med. Chem. 18 (2018) 9–25, https://doi.org/10.2174/1389557517666170807123201.
[21] V. Garima, F.K. Mohemmed, A. Wasim, A. Mohammad Mumtaz, A. Mymoona, S. Mohammad, A review exploring therapeutic worth of 1,3,4-oxadiazole tailored compounds, Mini Rev. Med. Chem. 19 (2019) 477–509, https://doi.org/10.2174/1389557518666181015152433.
[22] K. Tokumaru, J.N. Johnston, A convergent synthesis of 1,3,4-oxadiazoles from acyl hydrazides under semiaqueous conditions, Chem. Sci. 8 (2017) 3187–3191, https://doi.org/10.1039/C7SC00195A.
[23] Y.-Y. Wu, W.-B. Shao, J.-J. Zhu, Z.-Q. Long, L.-W. Liu, P.-Y. Wang, Z. Li, S. Yang, Novel 1,3,4-Oxadiazole-2-carbohydrazides as prospective agricultural antifungal agents potentially targeting succinate dehydrogenase, J. Agric. Food Chem. 67 (2019) 13892–13903, https://doi.org/10.1021/acs.jafc.9b05942.
[24] P.-Y. Wang, M.-W. Wang, D. Zeng, M. Xiang, J.-R. Rao, Q.-Q. Liu, L.-W. Liu, Z.-B. Wu, Z. Li, B.-A. Song, S. Yang, Rational optimization and action mechanism of novel imidazole (or imidazolium)-labeled 1,3,4-oxadiazole thioethers as

promising antibacterial agents against plant bacterial diseases, J. Agric. Food Chem. 67 (2019) 3535–3545, https://doi.org/10.1021/acs.jafc.8b06242.
[25] Z. Yang, P. Li, Y. He, J. Luo, J. Zhou, Y. Wu, L. Chen, Novel pyrethrin derivatives containing an 1,3,4-oxadiazole thioether moiety: design, synthesis, and insecticidal activity, J. Heterocycl. Chem. 57 (2020) 81–88, https://doi.org/10.1002/jhet.3750.
[26] S.A.M. Bouwman, R. Zoleko-Manego, K.C. Renner, E.K. Schmitt, G. Mombo-Ngoma, M.P. Grobusch, The early preclinical and clinical development of cipargamin (KAE609), a novel antimalarial compound, Travel Med, Inf. Disp. 36 (2020) 101765, https://doi.org/10.1016/j.tmaid.2020.101765.
[27] L.R. Raposo, A. Silva, D. Silva, C. Roma-Rodrigues, M. Espadinha, P.V. Baptista, M.M.M. Santos, A.R. Fernandes, Exploiting the antiproliferative potential of spiropyrazoline oxindoles in a human ovarian cancer cell line, Bioorg. Med. Chem. 30 (2021) 115880, https://doi.org/10.1016/j.bmc.2020.115880.
[28] H.V. Patel, K.A. Vyas, S.P. Pandey, P.S. Fernandes, Facile synthesis of hydrazonyl halides by reaction of hydrazones with N-halosuccinimide-dimethyl sulfide complex, Tetrahedron 52 (1996) 661–668, https://doi.org/10.1016/0040-4020(95)00916-7.
[29] J.R. Hwu, C.C. Lin, S.H. Chuang, K.Y. King, T.-R. Su, S.-C. Tsay, Aminyl and iminyl radicals from arylhydrazones in the photo-induced DNA cleavage, Bioorg. Med. Chem. 12 (2004) 2509–2515, https://doi.org/10.1016/j.bmc.2004.03.037.
[30] K. Hisler, A.G.J. Commeureuc, S.-z. Zhou, J.A. Murphy, Synthesis of indoles via alkylidenation of acyl hydrazides, Tetrahedron Lett. 50 (2009) 3290–3293, https://doi.org/10.1016/j.tetlet.2009.02.060.
[31] Y. Takahashi, R. Matsuhashi, Y. Miura, N. Yoshioka, Magnetic interactions through a Nonconjugated framework observed in back-to-Back connected Triazinyl–Nitroxyl Biradical derivatives, Chem. Eur J. 24 (2018) 7939–7948, https://doi.org/10.1002/chem.201800163.
[32] A. Alizadeh, L. Moafi, A convenient 1,3-dipolar cycloaddition reaction for the synthesis of spirooxindoles and some other spirocompounds containing the 1,3,4-oxadiazole moiety, Helv. Chim. Acta 99 (2016) 457–461, https://doi.org/10.1002/hlca.201500515.
[33] A. Alizadeh, L. Moafi, Simple access to spirooxadiazole compounds containing a quinoxaline moiety using a nitrile imine intermediate generated in situ, Heterocycl. Commun. 23 (2017) 375–378, https://doi.org/10.1515/hc-2017-0084.
[34] D.S. Wishart, Y.D. Feunang, A.C. Guo, E.J. Lo, A. Marcu, J.R. Grant, T. Sajed, D. Johnson, C. Li, Z. Sayeeda, N. Assempour, I. Iynkkaran, Y. Liu, A. Maciejewski, N. Gale, A. Wilson, L. Chin, R. Cummings, D. Le, A. Pon, C. Knox, M. Wilson, DrugBank 5.0: a major update to the DrugBank database for 2018, Nucleic Acids Res. 46 (2018) D1074–d1082, https://doi.org/10.1093/nar/gkx1037.
[35] C. Spry, C. Macuamule, Z. Lin, K.G. Virga, R.E. Lee, E. Strauss, K.J. Saliba, Pantothenamides are potent, on-target inhibitors of Plasmodium falciparum growth when serum pantetheinase is inactivated, PLoS One 8 (2013), e54974, https://doi.org/10.1371/journal.pone.0054974.
[36] J.E. Rosling, M.C. Ridgway, R.L. Summers, K. Kirk, A.M. Lehane, Biochemical characterization and chemical inhibition of PfATP4-associated Na+-ATPase activity in Plasmodium falciparum membranes, J. Biol. Chem. 293 (2018) 13327–13337, https://doi.org/10.1074/jbc.RA118.003640.
[37] M.B. Jiménez-Díaz, D. Ebert, Y. Salinas, A. Pradhan, A.M. Lehane, M.-E. Myrand-Lapierre, K.G. O'Loughlin, D.M. Shackleford, M. Justino de Almeida, A.K. Carrillo, J.A. Clark, A.S.M. Dennis, J. Diep, X. Deng, S. Duffy, A.N. Endsley, G. Fedewa, W.A. Guiguemde, M.G. Gómez, G. Holbrook, J. Horst, C.C. Kim, J. Liu, M.C.S. Lee, A. Matheny, M.S. Martínez, G. Miller, A. Rodríguez-Alejandre, L. Sanz, M. Sigal, N.J. Spillman, P.D. Stein, Z. Wang, F. Zhu, D. Waterson, S. Knapp, A. Shelat, V.M. Avery, D.A. Fidock, F.-J. Gamo, S.A. Charman, J.C. Mirsalis, H. Ma, S. Ferrer, K. Kirk, I. Angulo-Barturen, D.E. Kyle, J.L. DeRisi, D.M. Floyd, R.K. Guy, (+)-SJ733, a clinical candidate for malaria that acts through ATP4 to induce rapid host-mediated clearance of Plasmodium, Proc. Natl. Acad. Sci. Unit. States Am. 111 (2014) E5455–E5462, https://doi.org/10.1073/pnas.1414221111.
[38] A.M. Lehane, M.C. Ridgway, E. Baker, K. Kirk, Diverse chemotypes disrupt ion homeostasis in the malaria parasite, Mol. Microbiol. 94 (2014) 327–339, https://doi.org/10.1111/mmi.12765.
[39] P.R. Gilson, R. Kumarasingha, J. Thompson, X. Zhang, J.S. Penington, R. Kalhor, H.E. Bullen, A.M. Lehane, M.G. Dans, T.F. de Koning-Ward, J.K. Holien, T.P. Soares da Costa, M.D. Hulett, M.J. Buskes, B.S. Crabb, K. Kirk, A.T. Papenfuss, A.F. Cowman, B.M. Abbott, A 4-cyano-3-methylisoquinoline inhibitor of Plasmodium falciparum growth targets the sodium efflux pump PfATP4, Sci. Rep. 9 (2019) 10292, https://doi.org/10.1038/s41598-019-46500-5.
[40] W.C. Van Voorhis, J.H. Adams, R. Adelfio, V. Ahyong, M.H. Akabas, P. Alano, A. Alday, Y. Alemán Resto, A. Alsibaee, A. Alzualde, K.T. Andrews, S.V. Avery, V.M. Avery, L. Ayong, M. Baker, S. Baker, C. Ben Mamoun, S. Bhatia, Q. Bickle, L. Bounaadja, T. Bowling, J. Bosch, L.E. Boucher, F.F. Boyom, J. Brea, M. Brennan, A. Burton, C.R. Caffrey, G. Camarda, M. Carrasquilla, D. Carter, M. Belen Cassera, K. Chih-Chien Cheng, W. Chindaudomsate, A. Chubb, B.L. Colon, D.D. Colón-López, Y. Corbett, G.J. Crowther, N. Cowan, S. D'Alessandro, N. Le Dang, M. Delves, J.L. DeRisi, A.Y. Du, S. Duffy, S. Abd El-Salam El-Sayed, M.T. Ferdig, J.A. Fernández Robledo, D.A. Fidock, I. Florent, P.V.T. Fokou, A. Galstian, F.J. Gamo, S. Gokool, B. Gold, T. Golub, G.M. Goldgof, R. Guha, W.A. Guiguemde, N. Gural, R.K. Guy, M.A.E. Hansen, K.K. Hanson, A. Hemphill, R. Hooft van Huijsduijnen, T. Horii, P. Horrocks, T.B. Hughes, C. Huston, I. Igarashi, K. Ingram-Sieber, M.A. Itoe, A. Jadhav, A. Naranuntarat Jensen, L.T. Jensen, R.H.Y. Jiang, A. Kaiser, J. Keiser, T. Ketas, S. Kicka, S. Kim, K. Kirk, V.P. Kumar, D.E. Kyle, M.J. Lafuente, S. Landfear, N. Lee, S. Lee, A.M. Lehane, F. Li, D. Little, L. Liu, M. Llinás, M.I. Loza, A. Lubar, L. Lucantoni, I. Lucet, L. Maes, D. Mancama, N.R. Mansour, S. March, S. McGowan, I. Medina Vera, S. Meister, L. Mercer, J. Mestres, A.N. Mfopa, R.N. Misra, S. Moon, J.P. Moore, F. Morais Rodrigues da Costa, J. Müller, A. Muriana, S. Nakazawa Hewitt, B. Nare, C. Nathan, N. Narraidoo, S. Nawaratna, K.K. Ojo, D. Ortiz, G. Panic, G. Papadatos, S. Parapini, K. Patra, N. Pham, S. Prats, D.M. Plouffe, S.-A. Poulsen, A. Pradhan, C. Quevedo, R.J. Quinn, C.A. Rice, M. Abdo Rizk, A. Ruecker, R. St Onge, R. Salgado Ferreira, J. Samra, N.G. Robinett, U. Schlecht, M. Schmitt, F. Silva Villela, F. Silvestrini, R. Sinden, D.A. Smith, T. Soldati, A. Spitzmüller, S.M. Stamm, D.J. Sullivan, W. Sullivan, S. Suresh, B.M. Suzuki, Y. Suzuki, S.J. Swamidass, D. Taramelli, L.R.Y. Tchokouaha, A. Theron, D. Thomas, K.F. Tonissen, S. Townson, A.K. Tripathi, V. Trofimov, K.O. Udenze, I. Ullah, C. Vallieres, E. Vigil, J.M. Vinetz, P. Voong Vinh, H. Vu, N.-a. Watanabe, K. Weatherby, P.M. White, A.F. Wilks, E.A. Winzeler, E. Wojcik, M. Wree, W. Wu, N. Yokoyama, P.H.A. Zollo, N. Abla, B. Blasco, J. Burrows, B. Laleu, D. Leroy, T. Spangenberg, T. Wells, P.A. Willis, Open source drug discovery with the malaria box compound collection for neglected diseases and beyond, PLoS Pathog. 12 (2016), e1005763, https://doi.org/10.1371/journal.ppat.1005763.
[41] E.L. Flannery, C.W. McNamara, S.W. Kim, T.S. Kato, F. Li, C.H. Teng, K. Gagaring, M.J. Manary, R. Barboa, S. Meister, K. Kuhen, J.M. Vinetz, A.K. Chatterjee, E.A. Winzeler, Mutations in the P-type cation-transporter ATPase 4, PfATP4, mediate resistance to both aminopyrazole and spiroindolone antimalarials, ACS Chem. Biol. 10 (2015) 413–420, https://doi.org/10.1021/cb500616x.
[42] S. Meister, D.M. Plouffe, K.L. Kuhen, G.M.C. Bonamy, T. Wu, S.W. Barnes, S.E. Bopp, R. Borboa, A.T. Bright, J. Che, S. Cohen, N.V. Dharia, K. Gagaring, M. Gettayacamin, P. Gordon, T. Groessl, N. Kato, M.C.S. Lee, C.W. McNamara, D.A. Fidock, A. Nagle, T.-g. Nam, W. Richmond, J. Roland, M. Rottmann, B. Zhou, P. Froissard, R.J. Glynne, D. Mazier, J. Sattabongkot, P.G. Schultz, T. Tuntland, J.R. Walker, Y. Zhou, A. Chatterjee, T.T. Diagana, E.A. Winzeler, Imaging of Plasmodium liver stages to drive next-generation antimalarial drug discovery, Science 334 (2011) 1372–1377, https://doi.org/10.1126/science.1211936.
[43] R. Capela, J. Magalhães, D. Miranda, M. Machado, M. Sanches-Vaz, I.S. Albuquerque, M. Sharma, J. Gut, P.J. Rosenthal, R. Frade, M.J. Perry, R. Moreira, M. Prudêncio, F. Lopes, Endoperoxide-8-aminoquinoline hybrids as dual-stage antimalarial agents with enhanced metabolic stability, Eur. J. Med. Chem. 149 (2018) 69–78, https://doi.org/10.1016/j.ejmech.2018.02.048.
[44] I.H.J. Ploemen, M. Prudêncio, B.G. Douradinha, J. Ramesar, J. Fonager, G.-J. van Gemert, A.J.F. Luty, C.C. Hermsen, R.W. Sauerwein, F.G. Baptista, M.M. Mota, A.P. Waters, I. Que, C.W.G.M. Lowik, S.M. Khan, C.J. Janse, B.M.D. Franke-Fayard, Visualisation and quantitative analysis of the rodent malaria liver stage by real time imaging, PLoS One 4 (2009), e7881, https://doi.org/10.1371/journal.pone.0007881.
[45] M. Prudêncio, M.M. Mota, A.M. Mendes, A toolbox to study liver stage malaria, Trends Parasitol. 27 (2011) 565–574, https://doi.org/10.1016/j.pt.2011.09.004.
[46] T.A. Halgren, Merck molecular force field. I. Basis, form, scope, parameterization, and performance of MMFF94, J. Comput. Chem. 17 (1996) 490–519. https://doi.org/10.1002/(SICI)1096-987X(199604)17:5/6<490::AID-JCC1>3.0.CO;2-P.
[47] T.A. Halgren, MMFF VI. MMFF94s option for energy minimization studies, J. Comput. Chem. 20 (1999) 720–729, https://doi.org/10.1002/(SICI)1096-987X(199905)20:7<720::AID-JCC7>3.0.CO;2-X.
[48] P.C. Hawkins, A.G. Skillman, G.L. Warren, B.A. Ellingson, M.T. Stahl, Conformer generation with OMEGA: algorithm and validation using high quality structures from the Protein Databank and Cambridge Structural Database, J. Chem. Inf. Model. 50 (2010) 572–584, https://doi.org/10.1021/ci100031x.
[49] P.C.D. Hawkins, A.G. Skillman, G.L. Warren, B.A. Ellingson, M.T. Stahl, Conformer generation with OMEGA: algorithm and validation using high quality structures from the protein databank and cambridge structural database, J. Chem. Inf. Model. 50 (2010) 572–584, https://doi.org/10.1021/ci100031x.
[50] P.C. Hawkins, A. Nicholls, Conformer generation with OMEGA: learning from the data set and the analysis of failures, J. Chem. Inf. Model. 52 (2012) 2919–2936, https://doi.org/10.1021/ci300314k.
[51] P.C.D. Hawkins, A.G. Skillman, A. Nicholls, Comparison of shape-matching and docking as virtual screening tools, J. Med. Chem. 50 (2007) 74–82, https://doi.org/10.1021/jm0603365.